

8-11-73
NASA CR-132753

Final Report

**SELECTED SOLAR ELECTRIC PROPULSION
AND BALLISTIC MISSIONS STUDIES**

F. I. Mann
J. L. Horsewood

(NASA-CR-132753) SELECTED SOLAR ELECTRIC
PROPULSION AND BALLISTIC MISSIONS STUDIES
Final Report (Analytical Mechanics
Associates, Inc.) 92 p HC \$6.75

CSSL 21C G3/28

N73-25826

Unclas
06232

FACIL
UT BRANCH

Report No. 73-3
Contract NAS5-21691
January 1973

ANALYTICAL MECHANICS ASSOCIATES, INC.
10210 GREENBELT ROAD
SEABROOK, MARYLAND 20801

ANALYTICAL MECHANICS ASSOCIATES, INC.
AEROSPACE TECHNOLOGY

TELEPHONE:
301 / 794-7500

10210 GREENBELT ROAD
SEABROOK, MARYLAND 20801
21 May 1973

Dr. Robert Farquhar
Code 551
NASA Goddard Space Flight Center
Greenbelt, Maryland 20771

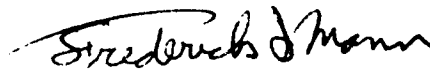
Re: Contract NAS5-21691

Dear Dr. Farquhar:

Enclosed are one hundred (100) copies of the Final Report for Contract NAS5-21691, "SELECTED SOLAR ELECTRIC PROPULSION AND BALLISTIC MISSIONS STUDIES", and ten (10) copies of the HILTOP User's Manual, "HILTOP: Heliocentric Interplanetary Low Thrust Trajectory Optimization Program". These constitute the last of the deliverable items for this contract.

It has been a pleasure working under you on the tasks of this contract, and I hope that the new mission data and performance analysis tools which have been created will be helpful to you for some time to come.

Sincerely,



Frederick I. Mann
Principal Investigator

FIM/bmf
Enclosures

cc: Mrs. Alice Vance, AMA, Inc., 50 Jericho, New York
Contracting Officer, Code 245, NASA Goddard Space Flight Center
Systems Reliability Directorate, Code 300, GSFC
T&DS Directorate, Code 500, GSFC
Patent Counsel, Code 204, GSFC
Documentation Branch, Code 256, GSFC ✓
GSFC Library, Code 252, GSFC

SUMMARY

This report documents the work carried out under contract NAS5-21691 to study selected missions using solar electric propulsion and conventional propulsion systems. The accomplishment of the contractual tasks required the extensive modification of the trajectory optimization computer program HILTOP. In addition to adding new program features, HILTOP was completely restructured to reduce execution time. The user's manual for the program was completely rewritten and is being published simultaneously with this report. The specific mission studies reported on are the direct and Venus swingby missions to the comet Encke and solar electric propulsion missions to Encke and to a distance of 0.25 AU from the sun.

TABLE OF CONTENTS

	<u>Page</u>
SUMMARY	i
I. INTRODUCTION	1
II. ANALYTICAL STUDIES	3
1. General Theory	4
2. Multiple Fixed Thrust Cone Angles	10
3. Solar Cell Performance Degradation	19
4. Spin Stabilized Spacecraft	24
5. The Multiple-Target Mission	29
III. NUMERICAL STUDIES	36
1. Direct Ballistic Encke Flyby Mission	36
2. Ballistic Flights to Encke Via Venus Swingby	38
3. SEP Encke Rendezvous Mission	40
4. Solar Electric Propulsion Solar Probe Mission	47
REFERENCES.....	52
FIGURES	53-57
TABLES	58-89

Preceding page blank

I. INTRODUCTION

During the last few years, large quantities of optimal solar electric propulsion (SEP) trajectory data have been generated, compiled and published, [1, 2, 3, 4, 5]. These data were prepared under a consistent set of guidelines and cover a large array of mission opportunities. Consequently, the data have proven valuable in defining appropriate applications for SEP and also in pointing out missions that are just as efficiently carried out with conventional propulsion systems.

Now that a number of missions have been identified as important and useful applications of solar electric propulsion, it is desired to examine these missions in much greater detail. Spacecraft design limitations, specific science objectives, trajectory estimation, navigation limitations, and guidance implementation are some of the considerations that have been largely ignored in the preliminary mission studies to date but which will, in the final analysis, have a major impact on mission and trajectory selection. The incorporation of these considerations in a mission analysis represents a major undertaking and requires a sophisticated set of computer software that is presently non-existent.

The purposes of this study were two-fold: (1) to extend the capabilities of the trajectory optimization program HILTOP for the more detailed mission studies and (2) to study selected cometary and solar probe missions. Both of these objectives have been achieved. The analyses performed to derive the extensions incorporated in the program are described in the following section and the numerical results of the missions studied are presented in the next section. A revised edition of the HILTOP user's manual is being published concurrently with this report.

Prior to commencing any program modifications, several potential extensions were considered and analyzed. These included multiple fixed-thrust directions, array orientation constraints, spin stabilized spacecraft, exponential

solar cell performance degradation, and multiple-target mission capability. Because of the complexity inherent in including any one of these program extensions, it became clear that an overhaul of HILTOP was mandatory if there were to be any hope of achieving a reasonably efficient and flexible program. This program overhaul was then undertaken, using as guidelines the known requirements of the several new features studied earlier. Although the available funds of the contract did not permit the inclusion of all features desired, the necessary groundwork was laid for their later inclusion with a minimum of effort. The multiple-target mission capability was given top priority and its incorporation in the program has been completed and checked out. In addition, much of the solar cell performance degradation has been included in the program. The restructuring of the program has had a significant effect on execution time. Through improved logical flow and more efficient coding, a reduction in machine time of about one-third was noted on several direct checks with the old version of the program.

The missions studied during the period of the contract include flyby and rendezvous missions to the comet Encke and solar probe missions. The comet Encke studies included ballistic flyby missions in the 1980 apparition, a ballistic flyby mission in 1980 using a Venus swingby, and a solar electric propulsion rendezvous mission arriving during the 1984 apparition. For the solar probe mission, solar electric propulsion was employed to achieve a solar distance of 0.25 AU. Flight profiles of $1\frac{1}{2}$, $2\frac{1}{2}$ and $3\frac{1}{2}$ revolutions were considered, and the penalties associated with fixed thrust angle and fixed reference power were assessed.

II. ANALYTICAL STUDIES

Much of the optimum trajectory and performance data generated to date for low thrust missions have been based on rather idealized assumptions regarding the control and performance of the propulsion system. This simplification was necessary and useful as it permitted the definition of general trends and approximate performance estimates with a minimum cost. Now that specific missions have been identified for further study, however, it is desired to incorporate in the studies those known or anticipated technology and hardware limitations that are expected to significantly affect performance and operational requirements.

Hardware and other limitations are introduced in trajectory analysis and optimization problems as constraints which greatly complicate the formulation and method of solution. Consequently, it is necessary to exercise care in incorporating constraints into a trajectory optimization code such as HILTOP to assure that the result is both reliable and efficient. The analysis of several potentially desirable constraint features in HILTOP was performed during the period of the contract. Among these were multiple fixed thrust cone angles, solar cell degradation, spin stabilized spacecraft and multiple target missions. The results of these analyses represent the basic analytic groundwork required to incorporate the features in HILTOP. The diversity and complexity of results indicated that a complete revision of the HILTOP is required to satisfactorily include most or all of these features. Consequently, the program was completely rewritten to speed the execution as well as to provide the necessary framework within which the constraint features may be incorporated. The multiple target capability was then identified as the most important and presently needed feature, and this capability was included in the revised program and checked out. Following are the analyses of each of the potential constraint features studied.

1. General Theory. To provide a base from which individual constraints may be considered, a general framework for the trajectory optimization problem is presented here. We start with the statement of the equations of motion

$$\begin{aligned}\dot{\mathbf{V}} &= \ddot{\mathbf{R}} = a \bar{\mathbf{e}}_t - \frac{\mu}{r^3} \mathbf{R} \\ \dot{\mathbf{R}} &= \mathbf{V}\end{aligned}\tag{1}$$

where \mathbf{R} is the position vector, r is the magnitude of \mathbf{R} , \mathbf{V} is the velocity vector, μ is the gravitational constant of the sun, a is the magnitude of the thrust acceleration and $\bar{\mathbf{e}}_t$ is a unit vector in the direction of thrust. In the discussions to follow, an upper case symbol will denote a vector, a lower case symbol will denote a scalar, and a lower case symbol with a bar will denote a unit vector. The thrust acceleration a is a function of several variables and may be written as follows:

$$a = h_{\sigma} \frac{g \gamma}{\nu}$$

where g is a reference thrust acceleration evaluated under a prescribed set of conditions, h_{σ} is a step function used in the formulation as a control variable for switching the engine on or off, ν is the ratio of current to initial mass, and γ is a power profile function which permits the description of the effect on power of various influences. As an example, for nuclear electric propulsion with no power degradation, γ would assume the constant value of one. For SEP, γ may assume a number of forms depending upon the assumptions made in modelling the problem. If the array is oriented normal to the sun at all times, then $\gamma = \gamma(r)$; if, on the other hand, the arrays are tilted an angle θ from the normal position, then $\gamma = \gamma(r, \theta)$. The function γ may also vary with time if power degradation is considered. For NEP, g is taken to be the thrust acceleration at the initial time; for SEP, it is evaluated as the thrust derived at 1 AU from the sun with arrays normal to the sun line, divided by the initial

spacecraft mass. The mass ratio satisfies the differential equation

$$\dot{\nu} = -h_{\sigma} \frac{g\gamma}{c}, \quad (2)$$

using $\nu = 1$ as an initial condition, where c is the jet exhaust speed which is assumed to be constant over the trajectory. Although both g and c are constants, it is useful to define them as state variables satisfying the differential equations

$$\begin{aligned} \dot{g} &= 0 \\ \dot{c} &= 0 \end{aligned} \quad (3)$$

so that they may be optimized using standard variational techniques. Other variables that are important under certain conditions are the propulsion time τ , defined by

$$\dot{\tau} = h_{\sigma} \quad (4)$$

where h_{σ} equals 1 when the thrusters are operating and zero otherwise, and the time from launch, $s = t - t_0$, which satisfies the differential equation

$$\dot{s} = 1 \quad (5)$$

The equations (1) - (5) constitute a set of state equations that are sufficiently general for many problems of interest. In fact, certain of these can be disregarded for certain problems. For instance, (4) is not necessary if the total propulsion time is unconstrained and (5) is not necessary if no solar cell degradation is considered. On the other hand, some problems will require the inclusion of additional state variables and equations. Examples of this will be seen subsequently in the problem of fixed thrust angles.

For generality at this point we will admit the possibility of constraints involving the state and control variables. These constraints will be denoted Ψ (a vector) and will be of the form

$$\Psi(R, U) = 0 \quad (6)$$

where U denotes a subset of the control variables. The state dependence of Ψ on position only is adequate to cover all the problems under consideration here.

The application of the Maximum Principle requires the introduction of a set of variables which are adjoint to the state variables. We denote λ_x as the variable adjoint to a state variable x . Then the scalar known as the variational Hamiltonian h_V is formed

$$h_V = \Lambda_V \cdot \dot{V} + \Lambda_R \cdot \dot{R} + \lambda_\nu \dot{\nu} + \lambda_\tau \dot{\tau} + \lambda_s \dot{s} + \lambda_g \dot{g} + \lambda_c \dot{c} + \Lambda_\Psi \cdot \Psi \quad (7)$$

which is employed to generate the differential equations for the adjoint variables

$$\dot{\lambda}_x = - \partial h_V / \partial x \quad (8)$$

Substituting (1) - (6) into (7) and then applying the general equation (8) yields

$$\begin{aligned} \dot{\Lambda}_V &= - \Lambda_R \\ \dot{\Lambda}_R &= \frac{\mu}{r^3} \Lambda_V - \frac{3\mu}{r^5} (R \cdot \Lambda_V) R - h_\sigma \frac{gR}{\nu r} (\Lambda_V - \frac{\nu}{c} \lambda_\nu) \frac{\partial \gamma}{\partial r} - \Lambda_\Psi \cdot \frac{\partial \Psi}{\partial R} \\ \dot{\lambda}_\nu &= h_\sigma \frac{g\gamma}{\nu^2} (\Lambda_V \cdot \bar{e}_t) \\ \dot{\lambda}_g &= - h_\sigma \frac{\gamma}{\nu} (\Lambda_V \cdot \bar{e}_t - \frac{\nu}{c} \lambda_\nu) \\ \dot{\lambda}_c &= - h_\sigma \frac{g\gamma}{c^2} \lambda_\nu \\ \dot{\lambda}_s &= - h_\sigma \frac{g}{\nu} (\Lambda \cdot \bar{e}_t - \frac{\nu}{c} \lambda_\nu) \frac{\partial \gamma}{\partial s} \\ \dot{\lambda}_\tau &= 0 \end{aligned} \quad (9)$$

In the literature, the vector Λ_V is termed the primer vector. Hereafter, the subscript V will be dropped and, by virtue of its relationship to the primer, Λ_R will be replaced with the negative of the time derivative of the primer.

The control variables for the problem are the thrust direction \bar{e}_t and the switch step function h_σ . According to the Maximum Principle, these controls are chosen to maximize the variational Hamiltonian, subject to any constraints imposed by the conditions (6). To facilitate this, we re-write (7) after substituting equations (1) - (6).

$$h_v = h_\sigma \left[\frac{g\gamma}{\nu} (\Lambda \cdot \bar{e}_t - \frac{\nu}{c} \lambda_\nu) + \lambda_\tau \right] - \frac{\mu}{r^3} (\Lambda \cdot R) - \dot{\Lambda} \cdot \dot{R} + \lambda_s + \Lambda \cdot \dot{\Psi} \cdot \Psi \quad (10)$$

Depending upon the specific form of γ and Ψ , the optimal control may be determined by inspection or it may require solution by numerical iteration. At this point, we will simply note that if there are no constraints (6) and if γ is not a function of the control \bar{e}_t , then the optimal control is immediately written

$$\begin{aligned} \bar{e}_t &= \Lambda / \lambda \\ h_\sigma &= 1 \quad \text{if} \quad \frac{g\gamma}{\nu} (\Lambda \cdot \bar{e}_t - \frac{\nu}{c} \lambda_\nu) + \lambda_\tau > 0 \\ h_\sigma &= 0 \quad \text{if} \quad \frac{g\gamma}{\nu} (\Lambda \cdot \bar{e}_t - \frac{\nu}{c} \lambda_\nu) + \lambda_\tau < 0 \end{aligned} \quad (11)$$

where $\lambda = |\Lambda|$. The function

$$\sigma_r = \Lambda \cdot \bar{e}_t - \frac{\nu}{c} \lambda_\nu \quad (12)$$

is of special significance because it represents the classical switch function if propulsion time is unconstrained.

Certain state boundary conditions will be specified in the problems under consideration. For example,

$$\begin{aligned} \nu(t_0) &= 1 \\ s(t_0) &= 0 \\ \tau(t_0) &= 0 \end{aligned} \quad (13)$$

On the other hand, it is generally desired to leave certain other boundary conditions open to be optimized and determined as a part of the solution. For example, the initial position and velocity of the spacecraft for interplanetary missions may be written

$$\begin{aligned} R(t_o) &= P_o(t_o) \\ \dot{R}(t_o) &= \dot{P}_o(t_o) + V_{\infty_o} \end{aligned} \tag{14}$$

where $P_o(t_o)$ and $\dot{P}_o(t_o)$ are the position and velocity, respectively, of the launch planet at time t_o and V_{∞_o} is the hyperbolic excess velocity of the spacecraft provided by the launch vehicle. Obviously, there exists only one degree of freedom - launch date - for P_o , \dot{P}_o and R_o . However, $\dot{R}(t_o)$ depends also on V_{∞_o} which may be left totally unspecified, partially specified (such as in magnitude only), or totally specified. Thus, depending upon the specific problem under consideration, there will exist a number of boundary conditions to be determined as a part of the solution. This is accomplished through the use of transversality conditions.

Individual transversality conditions are derived from the general equation

$$d\pi + [\Lambda \cdot dV - \dot{\Lambda} \cdot dR + \lambda_{\nu} d\nu + \lambda_s ds + \lambda_{\tau} d\tau + \lambda_g dg + \lambda_c dc - h_{\nu} dt]_o^f = 0 \tag{15}$$

where π denotes the performance index which is assumed to be of the form

$$\pi = \pi(v_{\infty_o}, v_{\infty_f}, \nu_f, g, c, t_o, t_f) \tag{16}$$

with v_{∞_f} being the hyperbolic excess speed upon arrival at the target. Thus

$$d\pi = \pi_{v_{\infty_o}} dv_{\infty_o} + \pi_{v_{\infty_f}} dv_{\infty_f} + \pi_{\nu_f} d\nu_f + \pi_g dg + \pi_c dc + \pi_{t_o} dt_o + \pi_{t_f} dt_f \tag{17}$$

where π_x denotes $\partial \pi / \partial x$. Of course, the individual transversality conditions are obtained by equating to zero the coefficients of all independent differentials. Typical results obtained for interplanetary missions follow.

If launch excess velocity direction is unspecified:

$$\Lambda_o \times V_{\infty o} = 0 \quad (\text{i.e., } V_{\infty o} / v_{\infty o} = \pm \Lambda_o / \lambda_o) \quad (18)$$

If launch excess speed is unspecified:

$$\pi_{v_{\infty o}} - (\Lambda_o \cdot V_{\infty o}) / v_{\infty o} = 0 \quad \text{if reference power is unspecified} \quad (19)$$

$$\pi_{v_{\infty o}} - \frac{(\pi_g + \lambda_{g_f}) g}{m_o} \frac{dm_o}{dv_{\infty o}} - (\Lambda_o \cdot V_{\infty o}) / v_{\infty o} = 0 \quad \text{if reference power is fixed.} \quad (20)$$

If arrival excess velocity direction is unspecified:

$$\Lambda_f \times V_{\infty f} = 0 \quad (\text{i.e., } V_{\infty f} / v_{\infty f} = \pm \Lambda_f / \lambda_f) \quad (21)$$

If arrival excess speed is unspecified:

$$\pi_{v_{\infty f}} + (\Lambda_f \cdot V_{\infty f}) / v_{\infty f} = 0 \quad (22)$$

The final mass ratio is generally unspecified, leading to

$$\pi_{\nu_f} + \lambda_{\nu_f} = 0 \quad (23)$$

If reference thrust acceleration is unspecified and reference power is not fixed:

$$\pi_g + \lambda_{g_f} = 0 \quad (24)$$

If jet exhaust speed is unspecified and reference power is not fixed:

$$\pi_c + \lambda_{c_f} = 0 \quad (25)$$

If reference power is fixed, the latter two conditions are replaced with the single condition

$$\pi_c + \lambda_{c_f} - (\pi_g + \lambda_{g_f})g \left(\frac{1}{c} - \frac{\eta'}{\eta} \right) = 0 \quad (26)$$

where η is over-all propulsion system efficiency, assumed to be a function only of c , and $\eta' = d\eta/dc$. The initial values of λ_g and λ_c are zero.

If launch date is unconstrained:

$$\pi_{t_o} - \Lambda_o \cdot \ddot{P}_o + \dot{\Lambda}_o \cdot \dot{P}_o - \lambda_{s_f} + h_v = 0 \quad (27)$$

If the arrival date is unconstrained:

$$\pi_{t_f} + \Lambda_f \cdot \ddot{P}_f - \dot{\Lambda}_f \cdot \dot{P}_f + \lambda_{s_f} - h_v = 0 \quad (28)$$

If t_o and t_f are unspecified, but flight time is fixed, the two conditions (27) and (28) are replaced by the one condition represented by the sum of (27) and (28). The initial value of λ_s , like λ_g and λ_c may be set to zero.

If propulsion time is unspecified:

$$\lambda_\tau = 0 \quad (29)$$

The above constitutes the necessary conditions for a general optimum low thrust interplanetary trajectory assuming the thrust direction is unconstrained and assuming the power developed is not a function of the direction of thrust. We will now define the modifications to the necessary conditions arising from various constraints and/or problem extensions.

2. Multiple Fixed Thrust Cone Angles. Optimal trajectories with unconstrained thrust direction will frequently result in a thrust angle relative to the sun line that fluctuates over a wide range during the course of the trajectory. With SEP systems, for which the arrays are usually assumed to continuously face the sun, this requires a continual movement of the thrusters relative to the arrays, a requirement that is highly undesirable. For this reason the concept of operating the system with a fixed spacecraft array configuration is

of much interest. The capability of simulating this constraint has been available in HILTOP for some time. However, the performance penalty incurred in some missions with a single fixed cone angle is excessive, so the ability to define the performance sensitivity to a number of fixed angles is desired.

Consider the case of a solar electric spacecraft with solar array orientation defined by the unit vector \bar{n} and thrust in the direction of the unit vector \bar{e}_t , and suppose that \bar{e}_t is constrained to lie nominally at one of a number of specified cone angles ϕ_i , $i = 1, 2, \dots, k$, from \bar{n} . Also, for generality, admit the possibility that \bar{e}_t may lie anywhere within a cone of specified half angle η_i about the nominal directions defined by ϕ_i . (This provides for the possibility of thrust vectoring). This constraint may be expressed mathematically by the inequality

$$\psi_1 = (\cos^{-1} (\bar{e}_t \cdot \bar{n}) - \phi_i)^2 - \eta_i^2 \leq 0 \quad (30)$$

In addition, it may be desirable in certain cases to orient the solar arrays to continuously maintain maximum power output. This may be accomplished by imposing the constraint

$$\psi_2 = \bar{n} \cdot \bar{e}_r - 1 = 0 \quad \text{for } r \geq r_c \quad (31)$$

or

$$\psi_2 = \bar{n} \cdot \bar{e}_r - r^2/r_c^2 = 0 \quad \text{for } r < r_c$$

where $\bar{e}_r = R/r$ and r_c is the solar distance at which the temperature effect on solar arrays oriented normal to the sun line causes the power factor γ to peak at a maximum value.

To the state equations (1) - (5), we add for this problem the k equations

$$\dot{\phi}_i = 0, \quad i = 1, 2, \dots, k \quad (32)$$

These are included to yield associated adjoint variables which will appear in transversality conditions if it is desired to optimize the k cone angles.

The variational Hamiltonian for this problem is written

$$\begin{aligned}
 h_v = h_\sigma & \left[\frac{g\gamma}{\nu} (\Lambda \cdot \bar{e}_t - \frac{\nu}{c} \lambda_\nu) + \lambda_r \right] - \frac{\mu}{r^3} (\Lambda \cdot R) - \dot{\Lambda} \cdot \dot{R} + \lambda_s \\
 & + \lambda_{x_i} \left[(\cos^{-1}(\bar{e}_t \cdot \bar{n}) - \phi_i)^2 - \eta_i^2 \right] + \lambda_y (\bar{n} \cdot \bar{e}_r - \rho)
 \end{aligned} \tag{33}$$

where $\rho = r^2/r_c^2$ if $r < r_c$ and $\rho = 1$ otherwise. Of course, λ_{x_i} and/or λ_y are zero if the associated constraints are not imposed. The optimal control problem now is to choose \bar{e}_t , \bar{n} , and h_σ at each point along the trajectory so as to maximize h_v subject to the specified constraints. Since the last two terms in (33) never contribute to the magnitude of h_v , it is seen by inspection that h_v is maximized with respect to \bar{e}_t and \bar{n} by choosing \bar{e}_t as close to Λ as possible and choosing \bar{n} so as to make γ as large as possible. Of course, any constraints between \bar{e}_t and \bar{n} preclude choosing \bar{e}_t and \bar{n} independently; therefore, it is, in general, necessary to compromise in maximizing γ and $(\bar{e}_t \cdot \Lambda)$ individually in favor of maximizing the function $\gamma (\Lambda \cdot \bar{e}_t - \frac{\nu}{c} \lambda_\nu)$. This must be done by considering individual cases that may arise.

First, to consider the case for which the solar arrays orientation is constrained so as to produce maximum power output. Under this constraint one can consider maximizing h_v only after the constraint is satisfied, and maximizing h_v is equivalent to maximizing $(\Lambda \cdot \bar{e}_t)$ subject to the constraint. Let α denote the angle between R and Λ and let j denote the index of the currently optimum cone angle (the determination of which cone angle is currently optimum will be considered subsequently). Then, for $r > r_c$, the constraint of maximum power output requires that $\bar{n} = \bar{e}_r$, and the choice of \bar{e}_t which maximizes $(\Lambda \cdot \bar{e}_t)$, and therefore h_v , subject to the constraint is

$$\bar{e}_t = \begin{cases} \bar{e}_r \cos(\phi_j + \eta_j) + (\bar{m} \times \bar{e}_r) \sin(\phi_j + \eta_j) & \text{if } \alpha \geq \phi_j + \eta_j \\ \bar{e}_\lambda & \text{if } \phi_j - \eta_j < \alpha < \phi_j + \eta_j \\ \bar{e}_r \cos(\phi_j - \eta_j) + (\bar{m} \times \bar{e}_r) \sin(\phi_j - \eta_j) & \text{if } \alpha \leq \phi_j - \eta_j \end{cases} \quad (34)$$

where $\bar{e}_\lambda = \Lambda/\lambda$ and $\bar{m} = (R \times \Lambda)/|R \times \Lambda|$. For $r < r_c$, \bar{n} is constrained to lie on a cone of half-angle

$$\theta = \cos^{-1}(r^2/r_c^2) \quad (35)$$

about \bar{e}_r , and the optimal choice for \bar{e}_t is

$$\bar{e}_t = \begin{cases} \bar{e}_r \cos(\phi_j + \eta_j + \theta) + (\bar{m} \times \bar{e}_r) \sin(\phi_j + \eta_j + \theta) & \text{if } \alpha \geq \phi_j + \eta_j + \theta \\ \bar{e}_\lambda & \text{if } \phi_j - \eta_j - \theta < \alpha < \phi_j + \eta_j + \theta \\ \bar{e}_r \cos(\phi_j - \eta_j - \theta) + (\bar{m} \times \bar{e}_r) \sin(\phi_j - \eta_j - \theta) & \text{if } \alpha \leq \phi_j - \eta_j - \theta \end{cases} \quad (36)$$

while \bar{n} (which is not always unique) may be defined

$$\bar{n} = \begin{cases} \bar{e}_r \cos \theta + (\bar{m} \times \bar{e}_r) \sin \theta & \text{if } \alpha \geq \phi_j + \theta \\ \bar{e}_r \cos \theta + (\bar{m} \times \bar{e}_r) \sin \theta \cos \epsilon + \bar{m} \sin \theta \sin \epsilon & \text{if } \phi_j - \theta < \alpha < \phi_j + \theta \\ \bar{e}_r \cos \theta - (\bar{m} \times \bar{e}_r) \sin \theta & \text{if } \alpha \leq \phi_j - \theta \end{cases} \quad (37)$$

where $\epsilon = \cos^{-1}[(\cos \phi_j - \cos \theta \cos \alpha)/\sin \theta \sin \alpha]$. Note that equations (36) and (37) also hold for the case $r > r_c$ if one sets $\theta = 0$.

For the case in which \bar{n} is not constrained to continuously yield maximum power output of the arrays, the optimal control problem becomes one of

maximizing the function $\gamma (\bar{e}_\lambda \cdot \bar{e}_t - b)$ subject to the cone angle inequality constraint (30), where $b = \lambda_\nu \nu / c \lambda$. As in the preceding case, when $\phi_j - \eta_j - \theta < \alpha < \phi_j + \eta_j + \theta$ the quantities γ and $\bar{e}_\lambda \cdot \bar{e}_t$ may be maximized independently while satisfying the cone angle constraint by rotating \bar{n} out of the plane of R and Λ . When α is not within this interval, both \bar{n} and \bar{e}_t must lie in the plane of R and Λ and the maximization of $\gamma (\bar{e}_\lambda \cdot \bar{e}_t - b)$ may be taken with respect to a single parameter, say the angle δ between \bar{e}_λ and \bar{e}_t . This is accomplished by solving the equation

$$(\cos \delta - b) \frac{\partial \gamma}{\partial \delta} - \gamma \sin \delta = 0 \quad (38)$$

for δ subject to the condition

$$(\cos \delta - b) \frac{\partial^2 \gamma}{\partial \delta^2} - 2 \sin \delta \frac{\partial \gamma}{\partial \delta} - \gamma \cos \delta \leq 0 \quad (39)$$

to assure the function is maximized. The solution of the equation (38) for δ will, for most forms of γ , require an iterative technique. For our purposes, γ written in terms of δ is of the form

$$\gamma = \sum_{i=0}^4 a_i \left(\frac{\cos (\alpha - \phi_j - \eta_j - \delta)}{r^2} \right)^{((i+4)/4)} \quad (40)$$

so that

$$\frac{\partial \gamma}{\partial \delta} = \tan (\alpha - \phi_j - \eta_j - \delta) \sum_{i=0}^4 a_i \left(\frac{i+4}{4} \right) \left(\frac{\cos (\alpha - \phi_j - \eta_j - \delta)}{r^2} \right)^{((i+4)/4)} \quad (41)$$

A suggested approach to the solution of equation (38) is to employ a Newton's iteration with $\sin \delta$ as the independent variable, using as a first guess

$$\sin \delta = \frac{1-b}{2-b} \tan (\alpha - \phi_j - \eta_j) \quad (42)$$

Once the optimum value of $\sin \delta$ is obtained, form $\cos \delta = \sqrt{1 - \sin^2 \delta}$ and write

$$\begin{aligned} \bar{e}_t &= \bar{e}_\lambda \cos \delta - (\bar{m} \times \bar{e}_\lambda) \sin \delta \\ \bar{n} &= \bar{e}_t \cos (\phi_j + \eta_j) - (\bar{m} \times \bar{e}_t) \sin (\phi_j + \eta_j) \quad \text{if } \alpha > \phi_j + \eta_j + \theta \end{aligned} \quad (43)$$

or

$$\bar{n} = \bar{e}_t \cos (\phi_j - \eta_j) - (\bar{m} \times \bar{e}_t) \sin (\phi_j + \eta_j) \quad \text{if } \alpha < \phi_j - \eta_j - \theta$$

Of course, if $\phi_j - \eta_j - \theta < \alpha < \phi_j + \eta_j + \theta$, then

$$\begin{aligned} \bar{e}_t &= \bar{e}_\lambda \\ \bar{n} &= \bar{e}_r \cos \theta + (\bar{m} \times \bar{e}_r) \sin \theta \cos \epsilon + \bar{m} \sin \theta \sin \epsilon \end{aligned} \quad (44)$$

with

$$\epsilon = \begin{cases} 0 & \text{if } \alpha \geq \phi_j + \theta \\ \cos^{-1} \left[(\cos \phi_j - \cos \theta \cos \alpha) / \sin \theta \sin \alpha \right] & \text{if } \phi_j - \theta < \alpha < \phi_j + \theta \\ \pi & \text{if } \alpha \leq \phi_j - \theta \end{cases} \quad (45)$$

To determine which of the ϕ_i is optimum at any instant, assume that $\phi_1 < \phi_2 < \dots < \phi_k$, and suppose that, at this instant,

$$\phi_i + \eta_i + \theta < \alpha < \phi_{i+1} - \eta_{i+1} - \theta$$

Then j , the index of the optimum cone angle at that instant is

$$j = \begin{cases} i & \text{if } (\phi_{i+1} - \eta_{i+1} - \alpha) - (\alpha - \phi_i - \eta_i) > 0 \\ i+1 & \text{if } (\phi_{i+1} - \eta_{i+1} - \alpha) - (\alpha - \phi_i - \eta_i) < 0 \end{cases}$$

The switch from one cone angle to the other occurs when the difference vanishes.

Since h_v is linear in h_σ , the choice of h_σ is made as described in (11).

The adjoint equations are obtained formally through partial differentiation of the variational Hamiltonian. Those that differ from equations (9) are

$$\ddot{\Lambda} = \frac{3\mu}{r^5} (\Lambda \cdot R) R - \frac{\mu}{r^3} \Lambda + \frac{1}{r} \left[h_\sigma \frac{g\gamma'}{\nu} (\Lambda \cdot \bar{e}_t - \frac{\nu}{c} \lambda_\nu) + h_\rho \lambda_y \right] \left[\bar{n} - 3 (\bar{e}_r \cdot \bar{n}) \bar{e}_r \right] \quad (46)$$

$$\dot{\lambda}_{\phi_j} = 2\lambda_{x_j} \left[\cos^{-1} (\bar{e}_t \cdot \bar{n}) - \phi_j \right]; \quad \dot{\lambda}_{\phi_i} = 0 \quad \text{for } i \neq j$$

where

$$\gamma' = \frac{1}{r^2} \sum_{i=0}^4 a_i \left(\frac{i+4}{4} \right) \left(\frac{\bar{e}_r \cdot \bar{n}}{r^2} \right)^{i/4} \quad (47)$$

and

$$h_\rho = \begin{cases} 0 & \text{if } r > r_c \\ 1 & \text{if } r < r_c \end{cases} \quad (48)$$

The Lagrange multipliers λ_{x_i} and λ_y are determined by setting the variations in h_v resulting from independent variations in \bar{e}_t and \bar{n} , respectively, to zero. That is,

$$\left[h_\sigma \frac{g\gamma}{\nu} \Lambda - 2\lambda_{x_i} \frac{(\cos^{-1} (\bar{e}_t \cdot \bar{n}) - \phi_j)}{\sqrt{1 - (\bar{e}_t \cdot \bar{n})^2}} \bar{n} \right] \cdot \delta \bar{e}_t = 0 \quad (49)$$

$$\left\{ \left[h_\sigma \frac{g\gamma'}{\nu} (\Lambda \cdot \bar{e}_t - \frac{\nu}{c} \lambda_\nu) + \lambda_y \right] \bar{e}_r - 2\lambda_{x_i} \frac{(\cos^{-1} (\bar{e}_t \cdot \bar{n}) - \phi_j)}{\sqrt{1 - (\bar{e}_t \cdot \bar{n})^2}} \bar{e}_t \right\} \cdot \delta \bar{n} = 0 \quad (50)$$

Now, because the variation of a unit vector must be normal to the unit vector, it is clear that $\delta \bar{e}_t$ may be divided into two components - one along $(\bar{n} \times \bar{e}_t)$

and the other along $(\bar{\mathbf{n}} \times \bar{\mathbf{e}}_t) \times \bar{\mathbf{e}}_t$. Since variations in these two directions are independent, the equation containing $\delta \bar{\mathbf{e}}_t$ must be satisfied by the variation along each component independently. Substituting into (49) the variation along $\bar{\mathbf{n}} \times \bar{\mathbf{e}}_t$ and using the identity $\bar{\mathbf{n}} \cdot (\bar{\mathbf{n}} \times \bar{\mathbf{e}}_t) = 0$ leads to the result

$$\Lambda \cdot (\bar{\mathbf{n}} \times \bar{\mathbf{e}}_t) = 0 \quad (51)$$

which indicates that Λ , $\bar{\mathbf{n}}$ and $\bar{\mathbf{e}}_t$ are coplanar vectors. Then, substituting into (49) the variation along the second component yields the desired definition of λ_{x_i} . Employing the identities

$$\Lambda \cdot [(\bar{\mathbf{n}} \times \bar{\mathbf{e}}_t) \times \bar{\mathbf{e}}_t] = -(\bar{\mathbf{n}} \times \bar{\mathbf{e}}_t) \cdot (\Lambda \times \bar{\mathbf{e}}_t)$$

$$\bar{\mathbf{n}} \cdot [(\bar{\mathbf{n}} \times \bar{\mathbf{e}}_t) \times \bar{\mathbf{e}}_t] = -(\bar{\mathbf{n}} \times \bar{\mathbf{e}}_t) \cdot (\bar{\mathbf{n}} \times \bar{\mathbf{e}}_t) = -(1 - (\bar{\mathbf{e}}_t \cdot \bar{\mathbf{n}})^2)$$

$$\bar{\mathbf{m}} = (\bar{\mathbf{n}} \times \bar{\mathbf{e}}_t) / |\bar{\mathbf{n}} \times \bar{\mathbf{e}}_t|$$

yields for λ_{x_i}

$$\lambda_{x_j} = h_\sigma \frac{g\gamma}{\nu} \frac{\bar{\mathbf{m}} \cdot (\Lambda \times \bar{\mathbf{e}}_t)}{2[\cos^{-1}(\bar{\mathbf{e}}_t \cdot \bar{\mathbf{n}}) - \phi_j]} ; \lambda_{x_i} = 0 \quad \text{for } i \neq j \quad (52)$$

Note that the identity involving $\bar{\mathbf{m}}$ is valid only outside the interval

$$\phi_j - \eta_j - \theta < \alpha < \phi_j + \eta_j + \theta$$

but, since $\Lambda \times \bar{\mathbf{e}}_t$ becomes the null vector when α is within the interval, the above expression for λ_{x_j} is valid for all α .

Before defining λ_y recall that λ_y is non-zero only if the array orientation is constrained to yield maximum power output. Also note that λ_y appears only in the equation for $\bar{\Lambda}$ where it is multiplied by the step function h_ρ . Therefore, λ_y influences the problem only when the array orientation

constraint is imposed and when $r < r_c$, and we will confine the discussion of λ_y to cases where those conditions apply. Proceeding as with $\delta \bar{e}_t$, consider $\delta \bar{n}$ broken down into the two components along $(\bar{n} \times \bar{e}_t)$ and $[(\bar{n} \times \bar{e}_t) \times \bar{n}]$. Employing in (50) first the component along $(\bar{n} \times \bar{e}_t)$ and noting the identity $\bar{e}_t \cdot (\bar{n} \times \bar{e}_t) = 0$, one is left with the condition

$$\left[h_\sigma \frac{g\gamma'}{\nu} (\Lambda \cdot \bar{e}_t - \frac{\nu}{c} \lambda_\nu) + \lambda_y \right] \left[\bar{e}_r \cdot (\bar{n} \times \bar{e}_t) \right] = 0 \quad (53)$$

Now, where α is outside the interval

$$\phi_j - \eta_j - \theta < \alpha < \phi_j + \eta_j + \theta$$

\bar{e}_r , \bar{n} and \bar{e}_t are coplanar such that $\bar{e}_r \cdot (\bar{n} \times \bar{e}_t) = 0$, and no information is given about λ_y . However, when α is within the interval, \bar{n} is rotated out of the plane of R and \bar{e}_t , and λ_y is then defined by the relation

$$h_\sigma \frac{g\gamma'}{\nu} (\Lambda \cdot \bar{e}_t - \frac{\nu}{c} \lambda_\nu) + \lambda_y = 0 \quad (54)$$

It remains to define λ_y when α is outside the interval, and this is done by considering the component of $\delta \bar{n}$ along $(\bar{n} \times \bar{e}_t) \times \bar{n}$. Employing the identities

$$\bar{e}_t \cdot [(\bar{n} \times \bar{e}_t) \times \bar{n}] = (\bar{n} \times \bar{e}_t) \cdot (\bar{n} \times \bar{e}_t) = 1 - (\bar{e}_t \cdot \bar{n})^2$$

$$\bar{e}_r \cdot [(\bar{n} \times \bar{e}_t) \times \bar{n}] = (\bar{n} \times \bar{e}_t) \cdot (\bar{n} \times \bar{e}_r)$$

$$\bar{m} = (\bar{n} \times \bar{e}_t) / |\bar{n} \times \bar{e}_t|$$

and substituting in (50) for λ_{x_i} leads to the relation

$$h_\sigma \frac{g\gamma'}{\nu} (\Lambda \cdot \bar{e}_t - \frac{\nu}{c} \lambda_\nu) + \lambda_y = h_\sigma \frac{g\gamma'}{\nu} \frac{\bar{m} \cdot (\Lambda \times \bar{e}_t)}{\bar{m} \cdot (\bar{n} \times \bar{e}_r)} \quad (55)$$

which completes the possible cases for which it is necessary to define λ_y .

As a final point, it should be noted that the transversality conditions to be satisfied if the k fixed cone angles ϕ_i are to be optimized are, simply,

$$\lambda_{\phi_i}(t_f) - \lambda_{\phi_i}(t_o) = 0; \quad i = 1, 2, \dots, k \quad (56)$$

where, without loss of generality, $\lambda_{\phi_i}(t_o)$ may be set to zero.

3. Solar Cell Performance Degradation. Solar radiation is known to degrade the performance of solar cells over long periods of time. Consequently, one may not expect the array output near the end of a mission to be as efficient as at the start. This time-varying performance is usually not simulated in trajectory studies because of the additional complexity and also because the nature of the performance decay is not that well known. The usual method of accounting for the effect is to estimate the power loss and increase the propulsion system mass proportionately. This is a conservative approach because it assumes the power lost is unavailable over the entire mission.

The radiation degradation model employed here assumes that the power decay is exponential in a parameter termed degradation time s . The specific formula used is

$$\gamma(r, \theta, s) = \gamma(r, \theta) e^{-s/\tau_d} \quad (57)$$

where τ_d is a specified constant representing the characteristic decay time, or time to decay to $1/e$ times its initial value, and $\gamma(r, \theta)$ is the power profile function as used in the preceding analyses. The assumed form of the function s will make a significant difference in both the nature of the decay and in the formulation of the solution. For example, if one assumes s to be simply the time from launch, then $\dot{s} = 1$ and the solution to the problem is contained within the general formulation presented earlier with

$$\frac{\partial \gamma}{\partial s} = - \frac{\gamma(r, \theta, s)}{\tau_d} \quad (58)$$

However, this is not felt to be a realistic assumption since it does not take into account the number of high energy particles impinging on the cells, which is a function of solar distance and array orientation. For the purposes of this analysis, we assume

$$\dot{s} = h_\sigma \frac{\bar{e}_r \cdot \bar{n}}{r^2} = h_\sigma \frac{\cos \theta}{r^2} = h_\sigma d \quad (59)$$

where d will be termed the density function, assumed to be non-negative. The coefficient h_σ is included because it is assumed the arrays will be oriented edgewise to the sun during coast phases to reduce the extent of decay. The density function d is proportional to the number of photons striking a unit area of arrays in a unit of time.

The variational Hamiltonian for this revised problem is

$$h_v = h_\sigma \left[\frac{g\gamma}{\nu} (\Lambda \cdot \bar{e}_t - \frac{\nu}{c} \lambda_\nu) + \lambda_s \frac{\bar{e}_r \cdot \bar{n}}{r^2} + \lambda_\tau \right] - \frac{\mu}{r^3} (\Lambda \cdot R) - \dot{\Lambda} \cdot R + \Lambda_\Psi \cdot \Psi \quad (60)$$

Thus, it is immediately evident that even this relatively simple power degradation model introduces rather profound changes in the nature of the solution. First, the thrust switch function (i.e., the term in square brackets multiplying h_σ) contains an additional term involving the adjoint variable λ_s . This implies that the degradation term can have a first-order effect in controlling the switch function and, consequently, the switching history may change significantly. Secondly, the appearance of the dot product $\bar{e}_r \cdot \bar{n}$ multiplying λ_s implies, except for when \bar{n} is constrained to lie along \bar{e}_r , that the degradation term will also have a direct and first-order effect on optimal control policy.

Denoting the term in square brackets in (60) as σ , the definition of the optimal choice of h_σ is

$$h_\sigma = \begin{cases} 1 & \text{if } \sigma > 0 \\ 0 & \text{if } \sigma < 0 \end{cases} \quad (61)$$

The choice of the optimal thrust direction depends upon the constraints, Ψ , of the problem under consideration. For the general problem posed previously with unconstrained thrust angle and arrays oriented to yield maximum instantaneous power, the optimal control policy remains unchanged from equations (11). It should be noted, however, that when $r < r_c$

$$d = \frac{\bar{e}_r \cdot \bar{n}}{r^2} \equiv \frac{1}{r_c^2} \quad (62)$$

if maximum instantaneous power output is to be maintained. The value of r_c is not affected by degradation when γ is given by equation (57). Of course, with degradation included in the simulation (i.e., $\tau_d < \infty$), the constraint of maximum instantaneous power output may be highly undesirable.

If the thrust direction is constrained to lie at fixed angles to \bar{n} , and \bar{n} is constrained for maximum instantaneous power output, then the optimal control policy including degradation remains unchanged from equations (34), (36), and (37). If, however, the directions of \bar{n} and \bar{e}_t are totally unconstrained, then the optimal control is determined by maximizing

$$\gamma(\bar{e}_\lambda \cdot \bar{e}_t - b) + qd \quad (63)$$

with respect to \bar{n} and \bar{e}_t independently, where $q = \lambda_s \nu / \lambda g$, and the other symbols are as defined earlier. Of course, the use of $\gamma = \gamma(r, \theta, s)$ is implied. This maximization is accomplished with respect to \bar{e}_t by inspection since γ , b , q and d are all independent of \bar{e}_t . That is, we choose

$$\bar{e}_t = \bar{e}_\lambda \quad (64)$$

The maximization with respect to \bar{n} is accomplished by solving iteratively for the value of d which satisfies

$$(1-b) \frac{\partial \gamma}{\partial d} + q = 0 \quad (65)$$

with

$$\frac{\partial \gamma}{\partial d} = e^{-s/\tau d} \sum_{i=0}^4 a_i \left(\frac{i+4}{4}\right) d^{1/4} \quad (66)$$

Using this value of d , one may then solve

$$\theta = \cos^{-1} (d r^2) \quad (67)$$

which represents the half-angle of a right circular cone about \bar{e}_r upon which \bar{n} must lie. The specific choice of \bar{n} on this cone is arbitrary and would probably be chosen to simplify control of the spacecraft.

Finally, if \bar{n} and \bar{e}_t are constrained to a set of fixed cone angles ϕ_i , the optimal control is determined by maximizing (63) with respect to a single variable, say the angle δ between \bar{e}_λ and \bar{e}_t . First, however, it is advisable to solve (65) for d and evaluate θ using (67). Then, if α , the angle between \bar{e}_r and \bar{e}_λ , is in the interval

$$\phi_j - \theta < \alpha < \phi_j + \theta$$

it is possible to maximize (63) with respect to \bar{n} and \bar{e}_t independently and satisfy the cone angle constraint by simply rotating \bar{n} out of the plane of \bar{e}_r and \bar{e}_λ . The optimal solution is then given by (44) using (45). If α is not within the specified interval, define $\theta = \alpha - \phi_j - \delta$, and solve the equation

$$(\cos \delta - b) \frac{\partial \gamma}{\partial \delta} - \gamma \sin \delta + q \frac{\partial d}{\partial s} = 0 \quad (68)$$

for δ subject to the condition

$$(\cos \delta - b) \frac{\partial^2 \gamma}{\partial \delta^2} - 2 \sin \delta \frac{\partial \gamma}{\partial \delta} - \gamma \cos \delta + q \frac{\partial^2 d}{\partial \delta^2} \leq 0 \quad (69)$$

with

$$\frac{\partial d}{\partial \delta} = \frac{\sin \theta}{r^2}; \quad \frac{\partial^2 d}{\partial \delta^2} = -\frac{\cos \theta}{r^2} = -d$$

$$\frac{\partial \gamma}{\partial \delta} = \frac{\partial \gamma}{\partial d} \frac{\partial d}{\partial \delta}$$

The equations for \bar{e}_t and \bar{n} are then given by (43) - (45) with η_j set to zero.

Partial differentiation of h_v as given by (60) yields the necessary adjoint equations. Of these, the only ones that differ from those of the preceding section are

$$\begin{aligned} \ddot{\Lambda} = & \frac{1}{r} \left[h_\sigma \frac{g\gamma'}{\nu} (\Lambda \cdot \bar{e}_t - \frac{\nu}{c} \lambda_\nu) + h_\sigma \frac{\lambda_s}{r^2} + h_\rho \lambda_y \right] \left[\bar{n} - 3(\bar{e}_r \cdot \bar{n}) \bar{e}_r \right] \\ & + \frac{3\mu}{r^5} (\Lambda \cdot R) R - \frac{\mu}{r^3} \Lambda \end{aligned} \quad (70)$$

$$\dot{\lambda}'_s = h_\sigma \frac{g\gamma}{\nu\tau_d} (\Lambda \cdot \bar{e}_t - \frac{\nu}{c} \lambda_\nu) \quad (71)$$

where γ' is given by

$$\gamma' = \frac{e^{-s/\tau_d}}{r^2} \sum_{i=0}^4 a_i \left(\frac{i+4}{4} \right) \left(\frac{\bar{e}_r \cdot \bar{n}}{r^2} \right)^{i/4} \quad (72)$$

The transversality conditions with solar cell degradation are modified only slightly from what was presented earlier. Since the final value of s is unspecified, we must have

$$\lambda_{s_f} = 0 \quad (73)$$

From (71) it is seen that λ_s is a non-decreasing function of time. Consequently, (73) implies that λ_s is a non-positive function throughout the trajectory, which tends to lower the value of the switch function and shorten the duration of powered phases.

The evaluation of the λ_{x_i} when including degradation effects proceeds exactly as in the preceding section and the results are as given in (52). The function λ_y is also obtained in the same manner as before; however, the degradation term in the variational Hamiltonian results in slightly different equations. The equation equivalent to (54), which defines λ_y if α is contained in the interval

$$\phi_j - \eta_j - \theta < \alpha < \phi_j + \eta_j + \theta$$

is

$$h_\sigma \left[\frac{g\gamma'}{\nu} (\Lambda \cdot \bar{e}_t - \frac{\nu}{c} \lambda_\nu) + \frac{\lambda_s}{r^2} \right] + \lambda_y = 0 \quad (74)$$

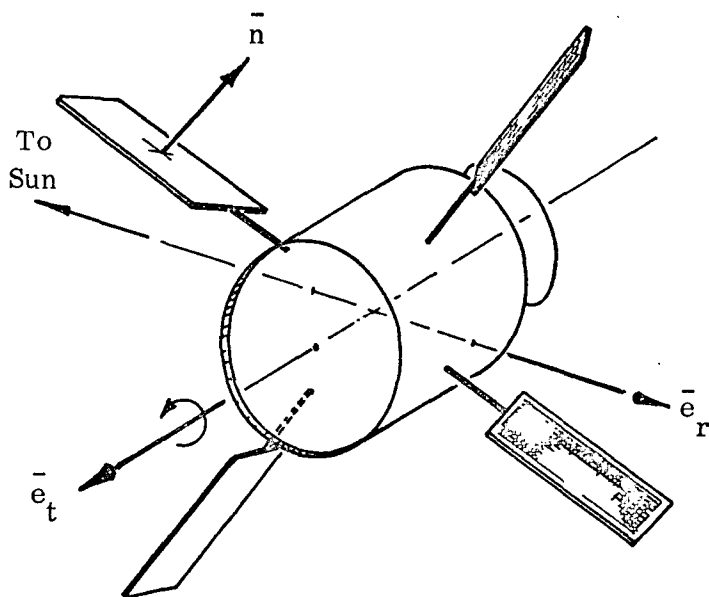
whereas the equation equivalent to (55), which holds for α outside the designated interval, is

$$h_\sigma \left[\frac{g\gamma'}{\nu} (\Lambda \cdot \bar{e}_t - \frac{\nu}{c} \lambda_\nu) + \frac{\lambda_s}{r^2} \right] + \lambda_y = h_\sigma \frac{g\gamma'}{\nu} \frac{\bar{m} \cdot (\Lambda \times \bar{e}_t)}{\bar{m} \cdot (\bar{n} \times \bar{e}_r)} \quad (75)$$

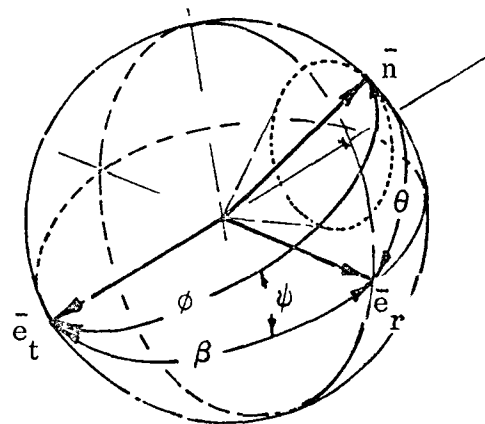
4. Spin Stabilized Spacecraft. Consider the case of a spinning solar electric spacecraft with thrust direction (coincident with the spin axis) defined by the unit vector \bar{e}_t . The solar cells are arranged on panels located symmetrically about the spin axis such that the normals to the arrays all have the same angular displacement from the spin axis at any instant in time. This angular displacement is denoted ϕ and shall be assumed constant throughout a trajectory. A spin stabilized spacecraft tends to maintain an inertially fixed attitude of the spin axis. Therefore, the thrust vector will also remain inertially fixed. For generality we shall permit the spin axis to assume any one of a prescribed number of inertial directions \bar{e}_{s_i} , $i = 1, 2, \dots, k$ at each instant in time with optimal switching among them.

For a spinner, the incidence angle of the photons impinging the arrays (and thus the output power of the arrays) varies over a revolution about the spin axis. Let the angle between the normal to the array and the sun line \bar{e}_r

at any instant in time be denoted θ . Then the density of photons impinging the solar array at that instant is linearly proportioned to $\cos \theta$, providing $\cos \theta$ is positive. If $\cos \theta$ is negative, then the cells are not exposed to the sun, and no power is generated. As the spacecraft rotates, the value of $\cos \theta$ continually changes causing a sinusoidal, or at least periodic, variation in the output power. But, since the period of spin is extremely short compared to the mission duration, we may effectively average the power generated over each cycle. The sketch (a) illustrates a typical conceptual SEP spacecraft configuration with four



(a) SEP spinner spacecraft



(b) Vector geometry

arrays placed symmetrically about the periphery, each oriented such that its normal \bar{n} is located at an angle ϕ to the spin axis. In sketch (b) is shown a typical geometrical arrangement of the pertinent vectors of the problem. During one revolution in spin, the vector \bar{n} moves once about the cone of half-angle ϕ centered on the spin axis. And, as \bar{n} transcribes the cone, the interior angle ψ goes through one complete revolution. Denoting the angle between \bar{e}_r and \bar{e}_t as β (i.e., $\cos \beta = \bar{e}_r \cdot \bar{e}_t$), it is seen that $\cos \theta$ is defined

$$\cos \theta = \cos \phi \cos \beta + \sin \phi \sin \beta \cos \psi \quad (76)$$

Now define the density function d

$$d = \begin{cases} \cos \theta / r^2 & \text{for } \cos \theta > 0 \\ 0 & \text{for } \cos \theta \leq 0 \end{cases} \quad (77)$$

We wish to average this function over one revolution in ψ . That is, we define the averaged d

$$\begin{aligned} d_{\text{ave}} &= \frac{1}{\pi r^2} \int_0^{\psi_{\text{lim}}} (\cos \phi \cos \beta + \sin \phi \sin \beta \cos \psi) d\psi \\ &= \frac{1}{\pi r^2} (\psi_{\text{lim}} \cos \phi \cos \beta + \sin \phi \sin \beta \sin \psi_{\text{lim}}) \end{aligned} \quad (78)$$

where

$$\psi_{\text{lim}} = \begin{cases} 0 & \text{if } \cos(\phi - \beta) < 0 \\ \cos^{-1}(-\cot \phi \cot \beta) & \text{if } \cos(\phi - \beta) > 0 > \cos(\phi + \beta) \\ \pi & \text{if } \cos(\phi + \beta) > 0 \end{cases} \quad (79)$$

Hereafter, we will drop the subscript ave from d and it shall be understood that the averaged value is implied. Also the subscript lim will be dropped when referring to the limiting value of ψ beyond which $\cos \theta$ is negative.

The equations of motion for this problem may be written

$$\dot{V} = \ddot{R} = h_{\sigma} \frac{g\gamma}{\nu} \bar{e}_t - \frac{\mu}{r^3} R$$

$$\dot{R} = V$$

$$\dot{\nu} = -h_{\sigma} \frac{g\gamma}{c}$$

$$\dot{g} = 0$$

$$\dot{c} = 0$$

(equation (80) continued on next page)

(80)

$$\begin{aligned}
\dot{\tau} &= h_{\sigma} \\
\dot{s} &= h_{\sigma} d \\
\dot{\phi} &= 0 \\
\dot{e}_{s_i} &= 0
\end{aligned}
\tag{80}$$

cont.

with γ defined

$$\gamma = e^{-s/\tau d} d \sum_{i=0}^4 a_i d^{i/4}
\tag{81}$$

and d , of course, is the value of the density function averaged over one revolution in ψ . The constraint that the thrust lie along one of the prescribed number of inertial directions may be written as the vector

$$\Psi = \bar{e}_t - \bar{e}_{s_j} = 0
\tag{82}$$

where \bar{e}_{s_j} denotes the current optimal choice of thrust direction. The variational Hamiltonian then becomes

$$\begin{aligned}
h_v = h_{\sigma} \left[\frac{g\gamma}{\nu} (\Lambda \cdot \bar{e}_t - \frac{\nu}{c} \lambda_{\nu}) + \lambda_s d + \lambda_{\tau} \right] - \frac{\mu}{r^3} (\Lambda \cdot R) - \dot{\Lambda} \cdot \dot{R} \\
+ \Lambda_{\Psi} \cdot (\bar{e}_t - \bar{e}_{s_j})
\end{aligned}
\tag{83}$$

and straightforward partial differentiation of h_v yields the adjoint equations

$$\begin{aligned}
\ddot{\Lambda} &= h_{\sigma} \left[\frac{g}{\nu} (\Lambda \cdot \bar{e}_t - \frac{\nu}{c} \lambda_{\nu}) \frac{\partial \gamma}{\partial d} + \lambda_s \right] \frac{\partial d}{\partial R} - \frac{\mu}{r^3} \Lambda + \frac{3\mu}{r^5} (R \cdot \Lambda) R \\
\dot{\lambda}_{\nu} &= -h_{\sigma} \frac{g\gamma}{\nu^2} (\Lambda \cdot \bar{e}_t) \\
\dot{\lambda}_g &= -h_{\sigma} \frac{\gamma}{\nu} (\Lambda \cdot \bar{e}_t - \frac{\nu}{c} \lambda_{\nu})
\end{aligned}
\tag{84}$$

(equation (84) continued on next page)

$$\dot{\lambda}_c = -h_\sigma \frac{g\gamma}{c^2} \lambda_\nu$$

$$\dot{\lambda}_\tau = 0$$

$$\dot{\lambda}_s = h_\sigma \frac{g\gamma}{\nu\tau_d} (\Lambda \cdot \bar{e}_t - \frac{\nu}{c} \lambda_\nu)$$

$$\dot{\lambda}_\phi = -h_\sigma \left[\frac{g}{\nu} (\Lambda \cdot \bar{e}_t - \frac{\nu}{c} \lambda_\nu) \frac{\partial \gamma}{\partial d} + \lambda_s \right] \frac{\partial d}{\partial \phi}$$

(84)
cont.

$$\dot{\Lambda}_{e_j} = \Lambda_\Psi; \quad \dot{\Lambda}_{e_i} = 0, \quad i \neq j$$

with

$$\frac{\partial \gamma}{\partial d} = e^{-s/\tau_d} \sum_{i=0}^4 a_i \left(\frac{i+4}{4} \right)_d^{i/4} \quad (85)$$

$$\frac{\partial d}{\partial \phi} = \frac{1}{\pi r^2} (\sin \beta \cos \phi \sin \psi - \psi \cos \beta \sin \phi) \quad (86)$$

$$\begin{aligned} \frac{\partial d}{\partial R} = \frac{1}{\pi r^3} \left\{ \frac{\sin \psi \sin \phi}{\sin \beta} \left[(1 - 3 \sin^2 \beta) \bar{e}_r - \cos \beta \bar{e}_t \right] \right. \\ \left. + \psi \cos \phi (\bar{e}_t - 3 \bar{e}_r \cos \beta) \right\} \quad (87) \end{aligned}$$

Since h_ν is linear in h_σ , the optimal choice of h_σ is clearly dependent upon the sign of σ , where

$$\sigma = \frac{g\gamma}{\nu} (\Lambda \cdot \bar{e}_t - \frac{\nu}{c} \lambda_\nu) + \lambda_s d + \lambda_\tau \quad (88)$$

That is

$$h_\sigma = \begin{cases} 1 & \text{if } \sigma > 0 \\ 0 & \text{if } \sigma < 0 \end{cases} \quad (89)$$

The selection of the current optimal inertial direction \bar{e}_{s_j} from the possible choices \bar{e}_{s_i} , $i = 1, \dots, k$ is made by a direct test of the magnitude of h_v resulting from the k possibilities. The direction yielding the largest value of h_v is assigned to \bar{e}_t .

The vector multiplier Λ_Ψ is evaluated by setting to zero the variation in h_v due to small changes in \bar{e}_t ; i.e.,

$$\left\{ h_\sigma \left[\frac{g\gamma}{\nu} \Lambda + \left(\frac{g}{\nu} (\Lambda \cdot \bar{e}_t - \frac{\nu}{c} \lambda_\nu) \frac{\partial \gamma}{\partial d} + \lambda_s \right) \frac{\partial d}{\partial \bar{e}_t} \right] + \Lambda_\Psi \right\} \cdot \delta e_t = 0 \quad (90)$$

where

$$\frac{\partial d}{\partial \bar{e}_t} = \frac{\bar{e}_r}{\pi r^2} (\psi \cos \phi - \sin \psi \sin \phi \cot \beta) \quad (91)$$

Since $\delta \bar{e}_t$ must be considered arbitrary, we set the term in curly brackets to zero, yielding

$$\Lambda_\Psi = -h_\sigma \left[\frac{g\gamma}{\nu} \Lambda + \left(\frac{g}{\nu} (\Lambda \cdot \bar{e}_t - \frac{\nu}{c} \lambda_\nu) \frac{\partial \gamma}{\partial d} + \lambda_s \right) \frac{\partial d}{\partial \bar{e}_t} \right] \quad (92)$$

Transversality conditions required in addition to those derived previously include those associated with the "best" choices of the k inertial vectors \bar{e}_{s_i} . The additional conditions are

$$\Lambda_{e_i}(t_f) = 0 \quad (93)$$

where, without loss of generality, the initial values of Λ_{e_i} were assumed zero.

5. The Multiple-Target Mission. The possibility exists of investigating more than one interplanetary target on a given space mission. Such missions are possible within the solar system using purely ballistic flight, with no thrust maneuvers whatever beyond the launch phase. The extension of purely ballistic missions to missions having a discrete set of high-thrust maneuvers along the trajectory increases the payload and versatility of a given mission, and also increases the complexity of the problem as viewed by the mission analyst,

whose lot it is to attempt to optimize some aspects of the overall mission subject to certain constraints. When continuous propulsion is permitted throughout space, as in the case of electric propulsion, the payload, mission versatility, and problem complexity generally increase even more, along with machine computation time and the difficulty of obtaining a numerical solution. Fortunately, most of the analytical groundwork required to describe an optimum electric propulsion multiple-target mission has already been covered by the single-target case. Specifically, all of the discussion relating to the Maximum Principle, which yields the optimal control variables along a trajectory, remains the same when extending a single-target mission to a multiple-target mission. The basic modification required is the extension of the analysis to include additional trajectory constraints and transversality conditions.

The mathematical discussion up to this point has involved only one target, which is designated the primary target, which stands apart from other possible targets in that it resides at the end of the trajectory of interest, by definition. Other targets in a multiple-target mission, which are designated intermediate-targets, must reside along the interior of a trajectory, after the launch planet and before the primary target. As will be evident below, the transversality conditions associated with an intermediate target are intrinsically different than those associated with the primary target, and this is basically because any possible trajectory extension beyond the primary target is ignored.

The introduction of intermediate targets along a trajectory gives rise to the possibility of dropping-off instrument packages at each such target, and the net spacecraft mass is assumed to satisfy this requirement at the primary target. Furthermore, the possibility of rendezvous with an intermediate target combined with the possibility of having Earth as a target downstream along the trajectory gives rise to the possibility of sample retrieval of material at an intermediate target, in other words, a sample-return mission.

Currently, the possible intermediate targets in the HILTOP program are restricted to be relatively massless celestial objects such as comets and asteroids. For the time being, the solution to the optimal multiple-target problem with massless targets and using electric propulsion is difficult enough, and very few numerical solutions are available in the literature. The possibility of massive intermediate targets, which give rise to gravitational perturbations of the trajectory, introduces many more degrees of freedom into the boundary value problem. A computer program called SWINGBY is available for investigating optimum electric propulsion missions involving one massive intermediate target, and this program is described in Reference [9]. In order to simulate a multiple-target mission using the HILTOP program, the ephemeris option, which is described in [10], must be used. The targets may be selected from the ephemeris library, or may be specified by inputting the orbital elements and relative perihelion times, or combinations thereof.

The analysis describing multiple-target missions will involve summations running from 1 to $n-1$, $\sum_{i=1}^{n-1}$, in which subscript 0 denotes the launch time and subscript n denotes the time of arrival at the primary target, which was previously denoted with subscript f . Therefore, subscripts $i = 1, 2, \dots, n-1$ denote the times at the intermediate targets. Subscript i , appearing without a summation, denotes the time at the i^{th} intermediate target.

The instrument package dropoff at the i^{th} intermediate target is described by the drop-mass $m_{\text{drop } i}$ through the drop-mass factor $k_{\text{drop } i}$ as follows:

$$m_{\text{drop } i} = m_o k_{\text{drop } i} \quad (94)$$

In like manner, the sample mass retrieved at the i^{th} intermediate target, $m_{\text{samp } i}$, is related to the sample-mass factor $k_{\text{samp } i}$:

$$m_{\text{samp } i} = m_o k_{\text{samp } i} \quad (95)$$

where m_o is the initial spacecraft mass. $k_{\text{drop } i}$ and $k_{\text{samp } i}$ are specified parameters and are available as independent variables to the boundary value problem, and $m_{\text{drop } i}$ and $m_{\text{samp } i}$ are available as dependent variables of the boundary value problem. This formulation leads to an increment in the mass ratio at the i^{th} intermediate target given by

$$\Delta \nu_i = k_{\text{samp } i} - k_{\text{drop } i} \quad (96)$$

The initial spacecraft mass is modified to include the drop-masses at all of the intermediate targets:

$$m_o = m_{\text{ps}} + m_p + m_t + m_s + m_r + m_{\text{net}} + m_o \sum_{i=1}^{n-1} k_{\text{drop } i} \quad (97)$$

and the propellant mass at the primary target becomes:

$$m_{\text{pn}} = m_o \left(1 - \nu_n + \sum_{i=1}^{n-1} (k_{\text{samp } i} - k_{\text{drop } i}) \right) \quad (98)$$

In the HILTOP program, stopover missions having optimum stopover time are simulated simply by forcing the spacecraft to rendezvous with the desired intermediate target. If the trajectory segment immediately following the intermediate-target arrival-time begins with a coast phase, then the duration of that coast phase is the optimum stopover time. If that trajectory segment begins with a thrust phase, then the optimum stopover time is zero. To simulate a stopover mission having a specified stopover time the same intermediate target should be specified twice consecutively, and of course the spacecraft should be forced to rendezvous with the intermediate target at the first encounter. Then inputting values for Λ and $\dot{\Lambda}$ at the start of the stopover trajectory segment (as boundary value problem independent variables) to be relatively small with respect to the mass ratio multiplier λ_ν will force the thrust switch function

to be negative and cause the spacecraft to coast along the intermediate target until the desired departure time is encountered. In this manner the trajectory block print and extrema of selected functions are available during the stopover phase.

The spacecraft position and velocity targeting conditions at an intermediate target are similar to those pertaining to the primary target. Denoting an intermediate target's position and velocity as P_i and \dot{P}_i , respectively, a constraint on the spacecraft position at an intermediate target is imposed by nulling the position error:

$$\Delta R_i = R_i - P_i = 0 \quad (99)$$

Similarly, a constraint on the spacecraft velocity \dot{R}_i at an intermediate target is imposed by nulling the velocity error:

$$\Delta \dot{R}_i = \dot{R}_i - \dot{P}_i - v_{\infty i} \frac{(\Lambda_i^+ - \Lambda_i^-)}{|\Lambda_i^+ - \Lambda_i^-|} \quad (100)$$

in which $v_{\infty i}$ is the excess speed at the i^{th} intermediate target and superscripts + and - refer respectively to times t_i^+ and t_i^- . Condition (100) makes use of the transversality condition which aligns the spacecraft excess velocity at the i^{th} intermediate target with the discontinuity in the primer. When condition (99) is imposed, the primer derivative $\dot{\Lambda}_i$ is generally discontinuous at the intermediate target under consideration, and $\dot{\Lambda}_i^+$ become three independent variables of the boundary problem, whereas Λ_i remains continuous. When condition (100) is imposed, the primer Λ_i itself is generally discontinuous at the i^{th} intermediate target, and Λ_i^+ become three more independent variables of the boundary value problem. The mass ratio adjoint variable λ_v remains continuous at an intermediate target.

The general equation for the transversality conditions expands to become

$$kd\pi + \sum_{i=1}^n \left[\Lambda_{\mathbf{x}} \cdot d\mathbf{X} - h_{\mathbf{v}} dt \right]_{t_{i-1}}^{t_i} = 0 \quad (101)$$

where \mathbf{X} denotes the vector of state variables of the problem. The convenient choice is made whereby λ_g and λ_c are forced to be continuous at each intermediate target, which means that, for example, only $\lambda_g(t_n)$ need appear in the derived transversality expressions rather than the cumbersome expression

$$\lambda_g(t_n) - \sum_{i=1}^{n-1} \left(\lambda_g^+(t_i) - \lambda_g^-(t_i) \right) - \lambda_g(t_0)$$

This is because $\lambda_g(t_n)$ alone, with $\lambda_g(t_0) = 0$ and $\lambda_g^+(t_i) = \lambda_g^-(t_i)$ for each i , has the same value as the cumbersome expression cited above if $\lambda_g(t_0)$ were not zero and $\lambda_g(t_i)$ were not continuous, and this is due to the absence of λ_g in the differential equations, the same being true for λ_c , and any other variable adjoint to a state variable that is a constant throughout the mission.

The performance index will still be of the functional form of (16). However, it is possible that the partials indicated in (17) may change slightly due to the inclusion of the drop and sample return masses. The actual form of all transversality conditions previously developed will remain unchanged. Additional conditions are introduced, however, relating to the conditions at the intermediate targets. If the velocity at an intermediate target is unconstrained

$$\Lambda_i^+ - \Lambda_i^- = 0 \quad (102)$$

That is, the primer is continuous if the velocity is unconstrained. The transversality condition yielding optimum encounter time at an intermediate target is

$$-(\Lambda_i^+ - \Lambda_i^-) \cdot \ddot{\mathbf{P}}_i + (\dot{\Lambda}_i^+ - \dot{\Lambda}_i^-) \cdot \dot{\mathbf{P}}_i + h_{\mathbf{v}}^+ - h_{\mathbf{v}}^- = 0 \quad (103)$$

The transversality condition yielding optimum launch date when the total flight is fixed is

$$\Lambda_n \cdot \ddot{P}_n - \dot{\Lambda}_n \cdot \dot{P}_n - h_{vn} - \Lambda_o \cdot \ddot{P}_o + \dot{\Lambda}_o \cdot \dot{P}_o + h_{vo} = 0 \quad (104)$$

III. NUMERICAL STUDIES

The specific missions investigated during the contract included ballistic flyby missions to the comet Encke in the 1980 apparition, both direct and via a Venus swingby, an Encke rendezvous mission in 1984 using solar electric propulsion, and a solar probe mission to 0.25 AU using solar electric propulsion. The results of each of these investigations are reported in the following paragraphs.

1. Direct Ballistic Encke Flyby Mission. The comet Encke currently holds much scientific interest as a potential source of new information regarding the source and nature of our solar system. Encke is one of the shortest period active comets, passing through perihelion once every 3.3 years, approximately. Consequently, it presents mission opportunities more frequently than most comets. It has a perihelion distance of about 0.34 AU and an aphelion of 4.1 AU. The orbit of Encke is inclined nearly 12 degrees to the ecliptic, and the line of apsides fortuitously is located only about five degrees from the line of nodes.

The 1980 apparition of comet Encke is of particular interest because of the exceptionally good Earth communication conditions that exist as Encke approaches perihelion. In Table 1 are presented the communication distance between Earth and Encke and the communication angle subtended at Earth between the Earth-sun line and the Earth-Encke line as a function of time from perihelion passage. It is seen that the minimum communication distance is about 0.273 AU which occurs 38 - 39 days prior to perihelion passage. Thereafter, the distance increases to about 1 AU at perihelion passage. Excellent viewing angles are available throughout the perihelion approach phase; sun interference should not begin until 20 days or so after perihelion passage.

Tabular listings of the orbital elements of the heliocentric transfer trajectories to Encke are shown as functions of launch date in Tables 2 - 5 for arrival dates of -10, 0, 10 and 20 days before perihelion, respectively. The parameters included in these tables are semi-major axis, eccentricity, inclination to the ecliptic, longitude of node measured from the Vernal Equinox, flight

path angle and speed at arrival, and aphelion and perihelion distances of the transfer conic.

In Tables 6 - 11, additional trajectory data are presented as a function of launch date for arrival dates of -10, 0, 10, 20, 30, and 40 days before perihelion, respectively. The trajectory parameters included are the Encke intercept speed, the launch hyperbolic excess speed and the departure asymptote declination relative to the Earth's equatorial plane. In addition, the payload delivered to the target using a Titan III D/Centaur/TE364(2250) launch vehicle is shown.

Desirable features of a ballistic flyby trajectory to Encke are: (1) slow intercept speed; (2) short flight time; (3) a reasonable launch vehicle payload which permits adequate scientific instrumentation, probably 500 - 700 kilograms; and (4) favorable intercept viewing conditions. Of these, it has already been noted that the intercept viewing conditions are favorable throughout the range of arrival dates considered. The launch vehicle payload is seen to fluctuate considerably as a function of launch date with the maximum capability increasing with earlier arrival dates. Nevertheless, for the selected launch vehicle, the payload capability shown exceeds the anticipated requirements over a sizeable range of launch dates for each arrival date included. The desirability of short flight times requires little or no compromising of other desirable features since the most favorable conditions are characteristics of the shorter flight time family of solutions. The most important parameter that tends to drive the selection of the launch and arrival dates is the target intercept speed. Considering the minimum intercept speed shown in Tables 6 - 11, it is seen that this parameter passes through an abrupt minimum for trajectories arriving near perihelion passage and flight times of about 100 days.

To more accurately define the minimum intercept speeds achievable, data were run on a finer grid. Trajectories were computed for arrival dates of -1, 0, and 1 days before perihelion at half-day increments in launch date around the nominal 100 day trajectory. These data are tabulated in Tables

12 - 14. It is seen that intercept speeds approaching 7 km/sec are available with trajectories arriving just after perihelion passage with flight times of about 102 days. Using the Titan III D/Centaur/TE364(2250) launch vehicle the payload capability exceeds 1000 kg which is well above the anticipated requirements. For comparison, the capability of the launch vehicle without the TE364 upper stage is about 550 kg for this trajectory.

The orbit for this mission is, in itself, quite interesting. The trajectory is nearly a Hohmann transfer, commencing near the line of ascending node of Encke's orbit and arriving near the descending node. This permits the spacecraft to be injected directly into the orbital plane of Encke. Consequently, the heliocentric velocities of the spacecraft and of Encke are nearly aligned at arrival such that the intercept speed is due solely to the difference in energies of the two orbits. The period of the spacecraft orbit is about 0.554 years. Consequently, the spacecraft will return very close to Earth five years from launch after traversing nine revolutions about the sun.

2. Ballistic Flights to Encke via Venus Swingby. Venus swingby trajectories to the comet Encke in the 1980 time period are available. An investigation of two distinct classes of solutions, however, failed to uncover any trajectories of immediate interest. One class of solutions was characterized by mission durations of about 370 days arriving at Encke 50 - 60 days prior to perihelion passage with intercept speeds of 27 - 30 km/sec. The second class of solutions was typically of 320 days duration arriving about twenty days after perihelion passage with intercept speeds of 30 - 33 km/sec. The second class of solutions does permit a reduction in launch excess speed to a value as low as 5.6 km/sec as compared to about 10 km/sec for the direct ballistic. This would permit an increase in payload or one conceivably could employ a smaller launch vehicle. The extremely high intercept speeds essentially render the solutions of no interest, however.

A set of tabular data for the second class of solutions is presented in Table 15. This table contains information for Earth launch dates between February 15 (2444285) and March 17, 1980 and Venus passage dates between July 17 (2444438) and July 31, 1980. At each grid point where a swingby solution exists with passage distance greater than 1 Venus radius, the values of three parameters are shown in the table. The upper value is the passage distance in Venus radii, the middle value is the launch hyperbolic excess speed in km/sec, and the last is the Venus-Encke leg flight time in days. Occasionally, two Venus-Encke trajectory legs are available and when this occurs the two solutions are separated with a slash.

The Venus swingby mode appears to be ill-suited for the 1980 Encke apparition due to unfavorable phasing of Venus and Encke. The greatest advantage of the swingby would be achieved if Venus' gravitational field could be employed to accomplish the plane change required to place the spacecraft in the orbital plane of Encke with a subsequent encounter of Encke at perihelion. To effect the necessary plane change requires a Venus encounter near the node of Encke's orbit on the orbital plane of Venus. This node is at an ecliptic longitude of about 320 degrees, a point which Venus passes about 140 days prior to perihelion passage by Encke. The transit to Encke through a 220 degree travel angle in a flight time of 140 days requires passing through an aphelion of about 1 AU. Hence, the trajectory following encounter of Venus is roughly the same conic as that of the best direct trajectory described in the preceding section. Thus, the best one could hope for using a Venus swingby in 1980 is an intercept speed near that of the direct mission. This could possibly be achieved with a smaller launch excess speed, but would require a much longer flight time (the spacecraft must first encounter Venus and return to about 1 AU before proceeding in to intercept Encke at perihelion).

An attempt was made to find a trajectory as described above. The date of July 19, 1980 was identified as the nodal passage date and was therefore

selected as the nominal swingby date. Earth-Venus trajectories which pass through perihelion prior to Venus encounter were selected as most probable candidates for the first trajectory leg. This restricted the Earth launch dates to be in the September-November 1979 time period leading to total flight times of about 430 days. For swingby dates of July 18 - 20, 1980, the smallest intercept speed found was over 9 km/sec, but this was not a valid solution because the required Venus passage distance was below the surface. Furthermore, the launch excess speed requirements for the solutions with low relative speeds at Encke were over 20 km/sec. Consequently, it was concluded that the existence of favorable Venus swingby trajectories to Encke in 1980 is doubtful.

3. SEP Encke Rendezvous Mission. It has been recognized for some time that SEP offers notable performance advantages for rendezvous missions to targets of negligible mass, such as a comet or asteroid. This advantage is multiplied if the orbit of the target has an energy level and/or ecliptic inclination that is greatly different from that of the Earth, as in the case of the comet Encke. These factors, in conjunction with the anticipated scientific potential of in situ monitoring of an active comet, have given much impetus to the study of an Encke rendezvous mission using SEP.

From a performance standpoint, the best rendezvous trajectories will arrive at Encke around the time of perihelion passage. This gives rise to the various launch opportunities that are characterized by the date of perihelion passage near the actual date of arrival (e.g., 1977, 1980, or 1984 missions). The actual time interval between opportunities, which is the period of Encke, is about 3.3 years. Probably the greatest amount of optimum trajectory data have been generated for the 1980 opportunity. Examples of this are to be found in References [3], [5] and [6] as well as in numerous other reports prepared in studies by JPL, TRW, North American Rockwell and IITRI. However, budgetary levels over the past few years have essentially precluded a rendezvous in 1980, so emphasis has now shifted to the 1984 opportunity for this

mission. A limited amount of information has been published on this opportunity. For example, Reference [3] contains data for optimum power levels over a large range of flight times arriving 50 days before perihelion passage assuming the Titan III D/Centaur launch vehicle, and References [7] and [8] contain data for fixed power levels and short flight time ranges.

The guidelines of this study were as follows:

- (1) consider the 1984 launch opportunity;
- (2) use the Titan III D/Centaur/TE364 (2250) launch vehicle;
- (3) assume a reference power level of 15 kilowatts and specific impulse of 3000 seconds;
- (4) arrive prior to perihelion passage, preferably as much as 50 days before; and
- (5) consider only short flight times so as to minimize spacecraft lifetime and reduce environmental hazards.

The consideration of flight time was determined to be particularly important because the most likely spacecraft to be available for the mission in the time frame of interest is the HELIOS. Since this spacecraft is being designed for ballistic solar probe missions of relatively short duration, the ability to extend the lifetime is an area of some concern. Because of this, it was decided to choose a mission duration as short as possible in the 18-24 month time period. This restricted the trajectory to a family of solutions that is generally characterized by travel angles in the approximate range of 180-270 degrees with the spacecraft proceeding immediately outward from Earth, passing through an aphelion of about 2.5 AU and finally rendezvousing with Encke as it approaches its perihelion.

The generation of optimal trajectory data for this mission proved to be particularly difficult under the guidelines specified. To begin the study, a 700 day solution was obtained which satisfied all the mission guidelines except that

arrival occurred at perihelion. Assuming a specific powerplant mass of 30 kg/kw, this solution yielded a net spacecraft mass of 703 kilograms, and exhibited no particular problems in converging. A sweep of the arrival date was then undertaken holding launch date fixed. At arrivals of 5, 10 and 15 days before perihelion, convergence was achieved very quickly. Thereafter, for earlier arrival dates, solutions became increasingly difficult to obtain. The earliest arrival date for which convergence was ultimately obtained was 24 days prior to perihelion passage with a net mass of 607 kilograms.

The technical problem in convergence arose because the iterator tended to drive the primer vector to near zero. This creates a sensitivity problem because a small change in one component results in a sizeable angular deviation in the vector and, hence, in the launch excess velocity which was aligned with the primer. Additionally the small value of the primer relative to its time derivative leads to very rapid angular rates of the thrust acceleration vector which causes numerical integration inaccuracies using normal integration intervals.

Upon closer study of a number of cases, all of which led to the vanishing initial primer under a variety of conditions, it was observed that there existed a certain amount of consistency in the initial direction and subsequent behavior of the primer vector. In each case it was noted that the primer rotated, in a very short period of time after launch (about 2 or 3 days) to a position nearly diametrically opposed to its initial position. Physically this implies that the early phases of the thrust program were being used to negate a portion of the effects of the launch excess velocity by thrusting in a direction opposite to the excess velocity. This condition was subsequently recognized to be important when combined with the result of a different approach to the problem.

The numerical difficulties gave rise to the possibility that a physical solution to the problem posed may not exist. To check this, it was postulated that there would then exist an earliest possible arrival date (i.e., a minimum

flight time for the specified launch date) for which the mission can be accomplished. Posing this as a problem in the calculus of variations gives the following transversality conditions (see equations 18, 20, and 23 of Section II):

$$\Lambda_o \times V_{\infty o} = 0$$

$$(\Lambda_o \cdot V_{\infty o})/v_{\infty o} + \lambda_g \frac{g}{m_o} \frac{dm_o}{dv_{\infty o}} = 0$$

$$\lambda_{\nu} = 0$$

where Λ_o is the initial primer vector, $V_{\infty o}$ is the launch excess velocity with magnitude $v_{\infty o}$, g is reference thrust acceleration, m_o is initial spacecraft mass, and λ_g and λ_{ν} are adjoint variables associated with g and mass ratio, respectively. Both λ_g and λ_{ν} are evaluated at the final time. The correct differential equations for λ_g and λ_{ν} are given earlier in Section II of this report (equations 9) which show that $\lambda_g \leq 0$ and $\lambda_{\nu} \geq 0$, where the equality applies only during coast phases. The last equation above, however, implies continuous thrusting throughout the mission, hence only the inequalities apply in this problem. Then, since λ_g is zero at time zero, one is assured that at the final time λ_g is negative. The first equation above implies that the initial primer and the launch excess velocity are collinear. Normally it is assumed that these two vectors are aligned. This choice is generally made on an intuitive basis and is believed to be correct usually. However, for this problem one will note that, since λ_g and $dm_o/dv_{\infty o}$ are negative and g and m_o are both positive, the only possible way in which the second transversality condition above can be satisfied is if $V_{\infty o}$ is opposed to Λ_o . Note that this is a general result for the minimum time problem with reference power fixed. Although no extensive literature survey was made, the authors are not aware of any publication in which this result was noted.

The above result gives credence to the possibility that a physical solution to the problem disappears as the flight time is reduced. Recall that the primer vector became very small, but stabilized in a condition such that shortly after launch it was directed nearly 180 degrees from its initial position. This had the effect of directing the thrust acceleration in the opposite direction as that of the launch excess velocity, which is precisely what the transversality conditions above dictate.

It is of interest to compare the transversality conditions of the original problem, that of maximum net spacecraft mass, with those derived above for minimum flight time. These may be written:

$$\Lambda_0 \times V_{\infty_0} = 0$$

$$(\Lambda_0 \cdot V_{\infty_0})/v_{\infty_0} + \lambda \frac{g}{m_0} \frac{dm_0}{dv_{\infty_0}} + [(1+k_t)\nu - k_t] \frac{dm_0}{dv_{\infty_0}} = 0$$

$$\lambda \nu - m_0 (1+k_t) = 0$$

where ν is the final mass ratio and k_t is the low thrust propellant tankage factor. The factor k_t was assumed to be 0.03 for this study. The first equation is again seen to require collinearity of Λ_0 and V_{∞_0} ; the second equation is identical to the corresponding condition for minimum time except for the addition of the third term on the left hand side; and the third condition requires the final value of $\lambda \nu$ to be positive definite, which implies that one cannot assume continuous thrust. The term within square brackets in the second equation is positive for reasonable values of ν and k_t ; consequently, the third term will be negative. The second term of this equation, however, is positive as discussed in the problem for minimum time. Therefore, the direction of V_{∞_0} relative to Λ_0 for the maximum net mass problem will depend on the relative magnitudes of the second and third terms of the second equation above. Replacing m_0 in favor of $\lambda \nu$ (through the third equation)

in the second term and forming the ratio

$$\rho = -\lambda_{\nu} [\nu - k_t / (1 + k_t)] / \lambda_g g,$$

which will always be positive, one may perform a simple test to determine the appropriate direction of V_{∞_0} relative to Λ_0 . This test is

$$V_{\infty_0} = v_{\infty_0} \Lambda_0 / \lambda_0 \quad \text{if } \rho > 1$$

$$V_{\infty_0} = -v_{\infty_0} \Lambda_0 / \lambda_0 \quad \text{if } \rho < 1$$

The case of $\rho = 1$ is a singularity for which Λ_0 assumes the null vector and there is sufficient information available to define the correct direction of V_{∞_0} .

To check the possibility that the solution disappears, the HILTOP program was modified to direct the launch excess velocity opposite the initial primer. With this change, a number of fixed arrival date trajectories were then generated for arrival dates prior to 25 days before perihelion passage. Not all of the pertinent transversality conditions were imposed, but the fact that solutions were obtained precluded the possibility that the optimal solution vanished. Once a solution for arrival at 50 days before perihelion passage was obtained, the remaining transversality conditions were imposed, and a fully optimum solution yielding a net mass of 280 kilograms was obtained. To observe the behavior of the solutions near the arrival date of 25 days before perihelion, where problems were experienced earlier, maximum net mass trajectories with launch excess velocity opposed to the primer were mapped as a function of arrival date. As the arrival date neared 25 days before perihelion, convergence became increasingly difficult to achieve. As before, this difficulty seemed to be related to the vanishing of the primer.

To better understand this problem, the function ρ was evaluated for each of the solutions obtained and is plotted as a function of arrival date in Figure 1. This curve exhibits a rather shallow, slightly negative, slope for arrivals of 0-17 days before perihelion. For these cases the solutions contain a single coast phase of nominally 80 days or less, occurring about 600 days into the mission. The abrupt change in slope at 17 days denotes the division between solutions with and without that coast phase. For earlier arrival dates, the value of ρ drops abruptly to near 1, and then quickly levels off and appears to approach 1 asymptotically. At still earlier arrival dates beyond the singularity, the value of ρ has dropped below 1 as it must if the reversal of $V_{\infty 0}$ relative to the initial primer is to be optimum. This portion of the curve is well behaved and remains near 1 throughout the interval of arrival dates shown.

Whether the two portions of the curve actually meet at a singularity or whether they each approach 1 asymptotically from their respective sides is presently unresolved. The answer is probably unimportant to anyone except those responsible for generating optimal trajectories who must resolve the cause of convergence difficulty or abandon the task when time has run out.

The maximum net spacecraft mass capability as a function of arrival date is presented in Figure 2. It is seen that the two segments of the curve could easily be joined with apparent continuity in both value and slope. This suggests that the physical aspects of the solution may be well behaved through the possible singularity. This possibility is supported by a close scrutiny of the characteristics of the solutions on each side of the singularity. Such a scrutiny indicated that the launch excess velocity directions were similar as were the thrust angles throughout the trajectory. Thus, any singularity is probably a mathematical singularity only; however, additional study is required to understand the cause.

A reasonable net spacecraft mass requirement for an early comet Encke rendezvous mission was estimated to be about 450 kilograms. From Figure 2 it is seen that this can be achieved using the Titan III D/Centaur/TE364 (2250) launch vehicle arriving at Encke 35 days before perihelion passage with a 665 day flight time. Some of the salient characteristics of this particular solution are presented in Table 16. Typical flight profiles for arrivals at perihelion and at 50 days prior to perihelion are shown in Figure 3.

4. Solar Electric Propulsion Solar Probe Mission. One of the missions for which solar electric propulsion offers a significant performance advantage over conventional propulsion systems is the solar probe mission. Performance data for close solar probes to 0.1 AU and 0.05 AU are available in the literature ^[3] for one mission mode. A major problem in performing a mission of this type is the limitations of a spacecraft and associated scientific equipment to withstand the severe environmental conditions concomitant with a close solar passage. There is, however, one spacecraft that is specifically designed to probe the solar environs. This is the HELIOS spacecraft which is capable of penetrating to 0.25 AU. Since this limit is well above the minimum distances studied previously, an analysis was undertaken to define the performance requirements for the 0.25 AU solar probe mission.

There exists a number of families of optimal electric propulsion solar probe trajectories to a given distance. These families are classified in terms of the central angle traversed, i.e., as $(n + \frac{1}{2})$ revolutions with $n = 0, 1, 2, \dots$. The family classed as $\frac{1}{2}$ revolution trajectory (i.e., $n = 0$) is the family containing the single impulse ballistic solution. This family is of little interest for SEP missions because the flight time is short and does not permit sufficient time for the electric propulsion system to effect a significant change in energy level. The families of solutions investigated here are the $1\frac{1}{2}$, $2\frac{1}{2}$ and $3\frac{1}{2}$ revolution trajectories. Typical flight profiles of these classes are shown in Figure 4. Although each profile shows the trajectory passing through successively smaller perihelion and aphelion distances each revolution of the sun, this will

not always be the case. Each profile shown represents a relatively short flight time for the corresponding trajectory class. To achieve this flight time with the specified travel angle, it is necessary to maintain a relatively small osculating semi-major axis throughout the trajectory. Any increase in flight time is accompanied with a corresponding increase in the osculating semi-major axis throughout the trajectory such that, for sufficiently long flight times, the aphelion distances of intermediate revolutions will substantially exceed 1 AU.

Although the direction of thrust is not indicated in the figures, it is essentially retrograde throughout the mission in all three classes. It was noted in earlier studies, however, that, for relatively long flight times within a class, the thrust profile tends to achieve the desired end conditions by increasing the eccentricity rather than by reducing the energy. This is accomplished by thrusting in a direction that is essentially fixed in inertial space and normal to the line of apsides.

The placement of coast phases in the trajectory profile is interesting and somewhat predictable. The conditions of optimality dictate that the solar probe trajectory always terminates in a coast phase. From past experience, it has been found that other coast phases may appear in a trajectory and that these will usually occur in the vicinity of a perihelion passage but biased to the approach side. Conversely, thrust phases are biased to the post-perihelion passage side. The $3\frac{1}{2}$ revolution trajectory profile is something of a curiosity in this regard. After starting the third revolution, the engine is shut down and the spacecraft coasts through a perihelion that is only slightly greater than the target radius. The coast period continues to near aphelion where a short powered phase establishes the necessary perihelion distance to achieve the specified target distance in the fourth revolution. Arrival at the specified distance is shown to occur in the vicinity of perihelion. Exceptions to this

condition do occur, as will be seen subsequently; however, these exceptions will generally not be of interest.

Specific solutions were obtained for selected flight times in each of the three families. The solutions were obtained for the Titan III D/Centaur/TE364 (2250) launch vehicle assuming a specific impulse of 3000 seconds and a specific propulsion system mass of 30 kg/kw. The reference power was optimized for each case. Several performance and trajectory parameters are tabulated as a function of flight time in Tables 17 to 19 for the $1\frac{1}{2}$, $2\frac{1}{2}$ and $3\frac{1}{2}$ revolution families, respectively. The data are tabulated at 10 day increments in flight time over the ranges of 160-250, 220-360, and 300-480 days for the short, medium and long central angle solutions, respectively.

A characteristic that holds for solutions in all three families is that as flight time is reduced, the distance at one or more intermediate perihelion passages decrease to values less than the target distance. This points to an inadequacy in the original problem definition in that the solution is required only to arrive at the specified distance at the specified time in each family of solutions. If, however, the desired distance is also reached at some point earlier in the mission, then the earlier achievement of the end condition would, in a practical sense, represent the culmination of the mission. This trajectory to the earliest achievement of the desired distance is not a fully optimum trajectory since all of the transversality conditions are not satisfied at that time. Consequently, the entire solution is likely to hold no practical interest. A perusal of the data in Tables 17 to 19 leads to the conclusion that only the longest flight time solution obtained for the $3\frac{1}{2}$ revolution class maintains all three perihelion passage distances above the target distance of 0.25 AU. Since longer flight times are questionable due to lifetime considerations of the HELIOS spacecraft, the $3\frac{1}{2}$ revolution class of solutions is considered to be an inappropriate choice for an early solar probe mission. Therefore, the remaining discussion will be limited to the $1\frac{1}{2}$ and the $2\frac{1}{2}$ revolution solutions. Due to

the perihelion passage distance limitation it is seen that the minimum flight times of interest for these two families of solutions are about 180 and 320 days, respectively.

The tabular data indicate that either family of solutions permit the placement of payloads in excess of 1500 kilograms on target using the specified launch vehicle and power levels of about 30 kilowatts. However, at the low launch excess speeds associated with the longer flight times within a class, the TE364 upper stage offers no payload advantage; consequently, the tabulated results for cases in which the excess speed is less than, say, 8 km/sec also apply for the Titan III D/Centaur vehicle without the upper stage. This may be compared with the capability of the Titan 3D/Centaur/TE364 (2250) launch vehicle with no SEP stage. This vehicle can place about 800 kilograms to the specified distance in about 90 days. This would imply, of course, that until there is a requirement for either a heavier spacecraft than HELIOS or a closer target distance than 0.25 AU, the Titan III D/Centaur/TE364 (2250) can perform the solar probe mission with no requirement for SEP. This is not, of course, a new revelation, since ballistic HELIOS missions using this launch vehicle are presently being studied.

A performance sensitivity study was performed to define the effects, relative to the data described above, of the following constraints:

- (1) reference power fixed at 15 kilowatts;
- (2) same as (1), but without TE364 upper stage; and
- (3) same as (1), but with optimum fixed thrust angle relative to the sun-spacecraft line.

Table 20 describes the code employed in tabulating the results of the sensitivity data in Tables 21 and 22. In these two tables, containing data for the $1\frac{1}{2}$ and $2\frac{1}{2}$ revolution solutions, respectively, are presented the performance and trajectory data for the optimum plus three constrained cases at four selected flight times.

One additional column is also provided to list the optimum power level and the optimum fixed thrust angle for each flight time. These data clearly show that, for the cases of primary interest for SEP, the penalties from any one or all of the three constraining conditions listed above are minimal. They also show that the sensitivities for the $1\frac{1}{2}$ revolution family are less than for the $2\frac{1}{2}$ revolution family.

REFERENCES

- [1] J. L. Horsewood and F. I. Mann, "Optimum Solar Electric Interplanetary Trajectory and Performance Data," NASA CR 1524, April 1970.
- [2] J. L. Horsewood and F. I. Mann, "Solar Electric Interplanetary Trajectory and Performance Data for Sub-Optimal Powered Spacecraft," NASA CR 112840, April 1970.
- [3] J. L. Horsewood, F. I. Mann and P. F. Flanagan, "Solar Electric Performance Data for Extra-Ecliptic and Solar Probes and Ceres, D'Arrest, and Encke Rendezvous Missions," NASA CR 118312, December 1970.
- [4] F. I. Mann and J. L. Horsewood, "Optimum Solar Electric Interplanetary Mission Opportunities from 1975 to 1990," AMA, Inc. Report No. 71-44, December 1971.
- [5] F. I. Mann and J. L. Horsewood, "A Study of the Applicability of Solar Electric Propulsion," AMA, Inc. Report No. 71-43, December 1971.
- [6] J. A. Gardner, "Solar Electric Propulsion System Integration Technology (SEPSIT) Final Report," Jet Propulsion Laboratory Technical Memorandum 33-583, November 1972.
- [7] "Extended Definition Feasibility Study for a Solar Electric Propulsion Stage," North American Rockwell Report No. SD72-SA-0177-1, Vol. 1 - Executive Summary, January 1973.
- [8] "Study of a Comet Rendezvous Mission," TRW Systems Report No. 20513-6005-RO-00, April 1972.
- [9] J. L. Horsewood and C. Hipkins, "SWINGBY: A Low Thrust Interplanetary Swingby Trajectory Optimization Program," Analytical Mechanics Associates, Inc., Report No. 71-10, March 1971.
- [10] F. I. Mann, J. L. Horsewood, and P. F. Flanagan, "HILTOP: Heliocentric Interplanetary Low Thrust Trajectory Optimization Program," Analytical Mechanics Associates, Inc., Report No. 73-1, January 1973.

FIGURES

Figure 1

1984 SEP ENCKE RENDEZVOUS MISSION

Transversality Ratio Behavior

Launch Date is April 27, 1982

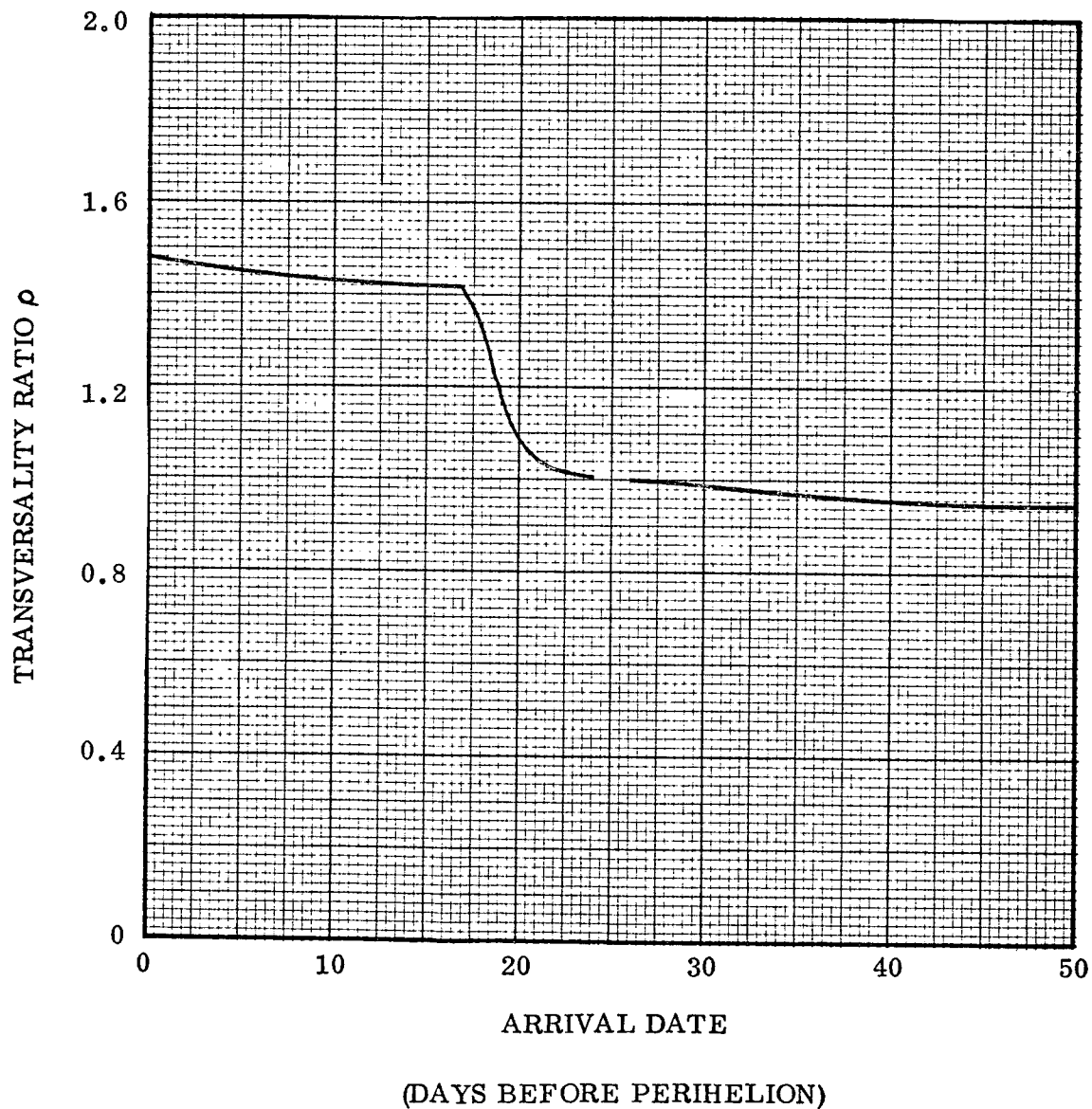


Figure 2

1984 SEP ENCKE RENDEZVOUS MISSION

Net Spacecraft Mass Capability

Launch Date is April 27, 1982

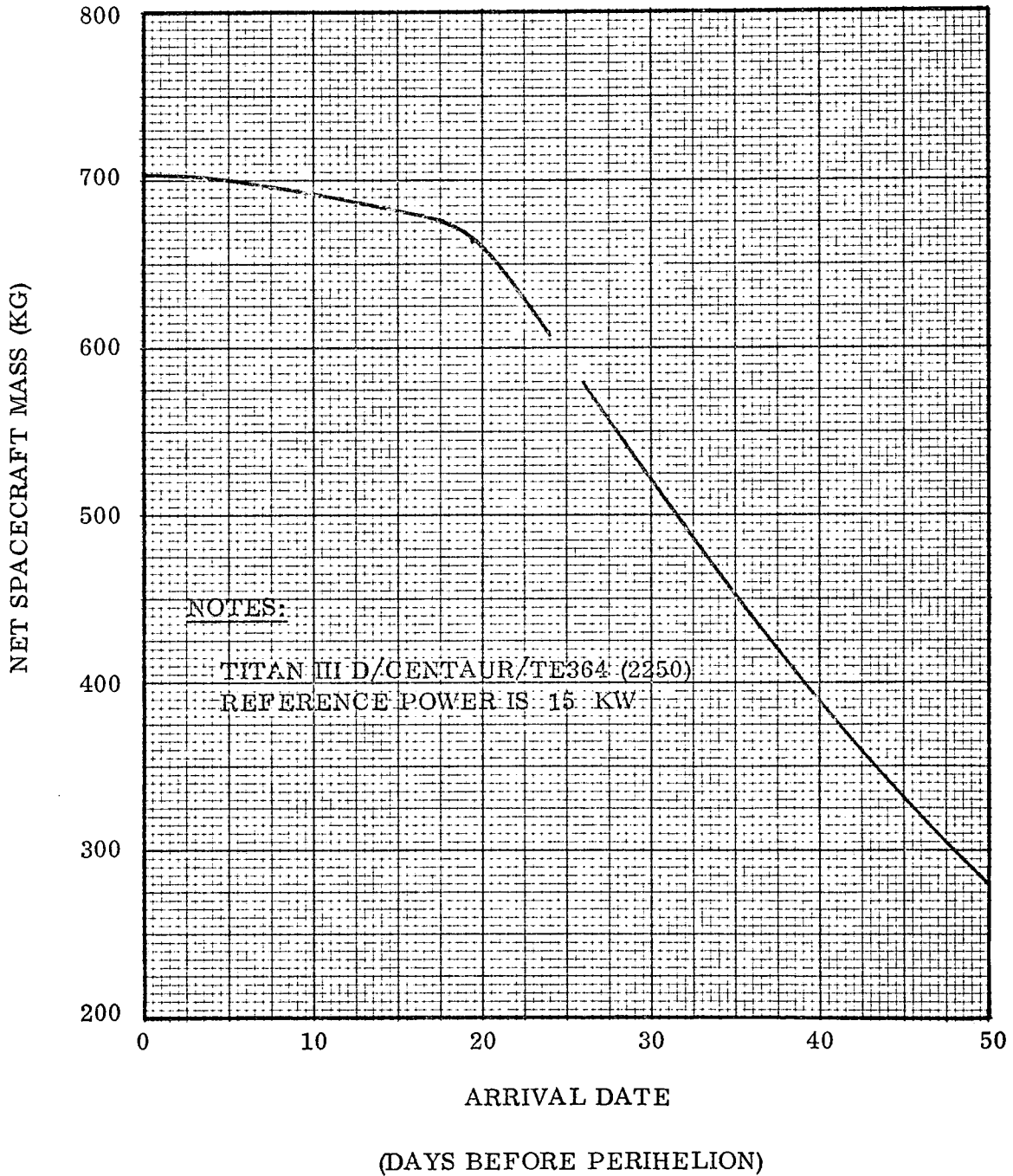


Figure 3

1984 SEP ENCKE RENDEZVOUS MISSION

Typical Flight Profiles

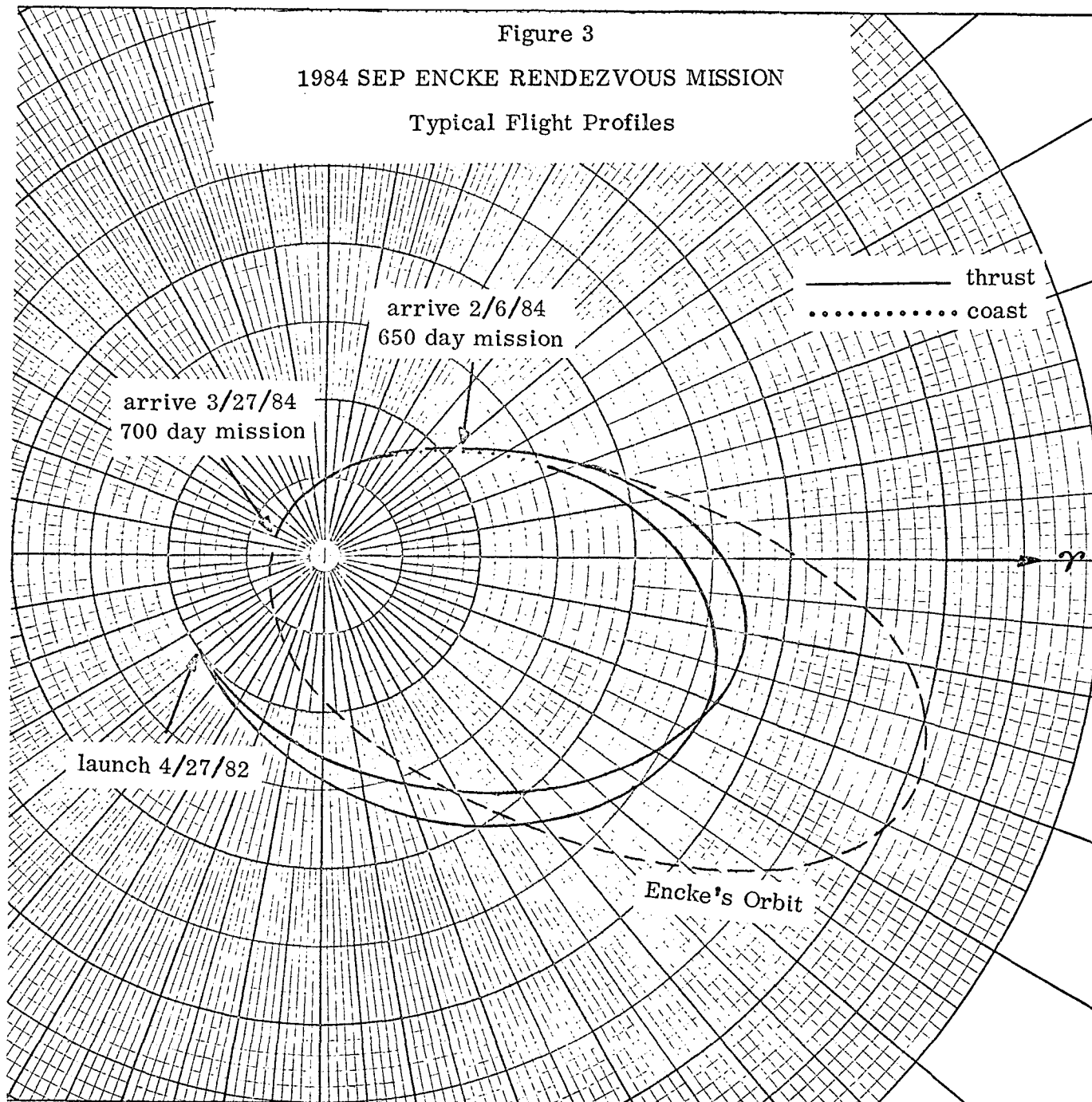
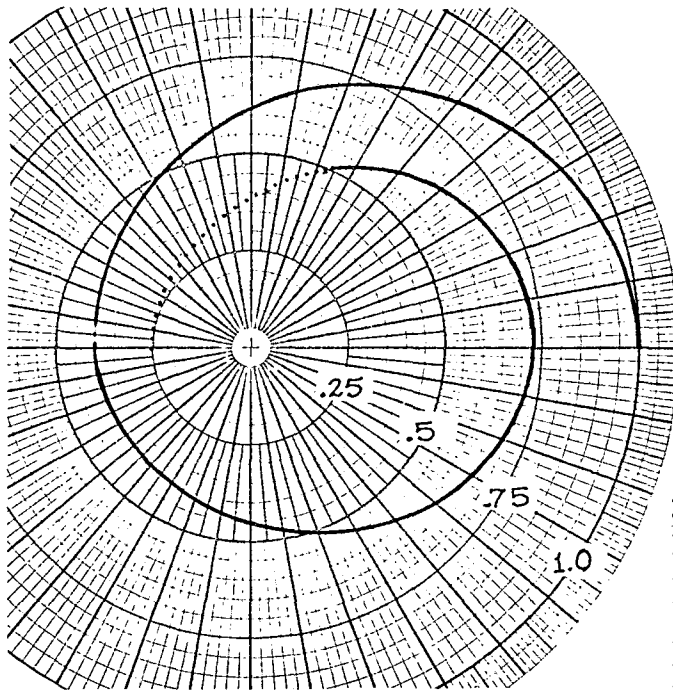


Figure 4

SEP SOLAR PROBE TRAJECTORY PROFILES



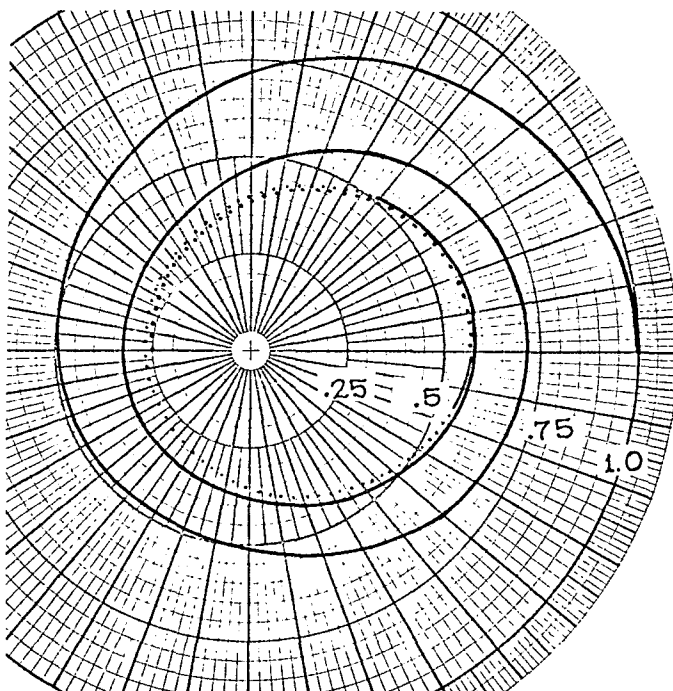
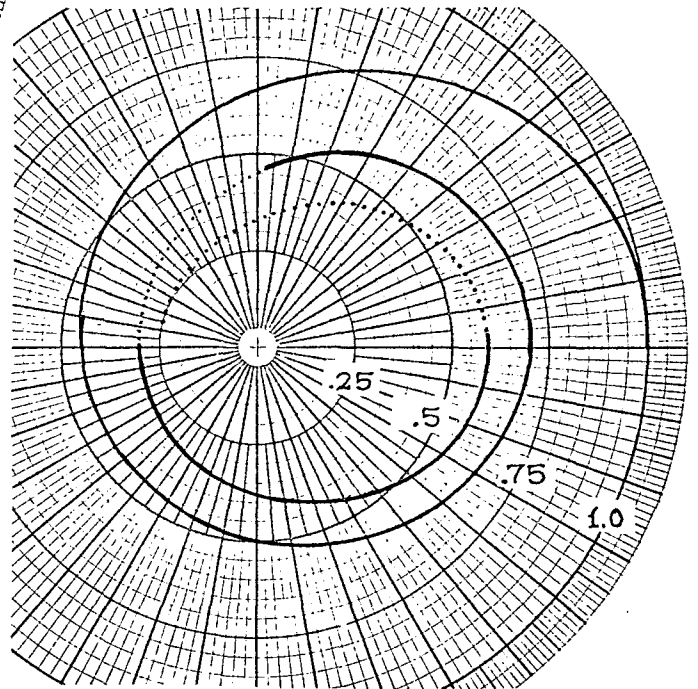
———— thrust

..... coast

(a) $1\frac{1}{2}$ revolutions, 250 days

Note: Distances are in AU.

(b) $2\frac{1}{2}$ revolutions, 360 days



(c) $3\frac{1}{2}$ revolutions, 480 days

TABLES

Table 1

STRAIGHT BALLISTIC MISSIONS TO ENCKE IN 1980
COMMUNICATION PARAMETERS AT INTERCEPT

Days Before Perihelion	Communication Distance (AU)	Communication Angle (DEG)
-10	1.296	14.5
0	1.001	19.7
10	0.699	22.9
20	0.473	28.2
30	0.321	44.9
35	0.281	59.7
36	0.277	63.0
37	0.274	66.5
38	0.273	70.0
39	0.273	73.5
40	0.274	76.9
41	0.277	80.3
42	0.281	83.6
43	0.287	86.7
44	0.293	89.6
45	0.301	92.4
46	0.309	95.0
47	0.319	97.4
50	0.353	103.3

Table 2

STRAIGHT BALLISTIC MISSIONS TO ENCKE IN 1980
ARRIVING 10 DAYS AFTER PERIHELION

Launch Date	Flight Time (Days)	Semi-Major Axis (AU)	Eccentricity	Inclination (DEG)	Node (DEG)	Final γ (DEG)	Final V (EMOS)	Aphelion (AU)	Perihelion (AU)
Nov. 6 (1980)	40	-1.214795	1.248327	56.321	44.2	35.088	2.339	∞	0.3017
Oct. 27	50	3.162539	0.908452	75.460	214.2	33.898	2.081	6.0356	0.2895
Oct. 17	60	1.147843	0.723564	40.463	204.3	27.826	1.943	1.9784	0.3173
Oct. 7	70	0.860263	0.612395	26.055	194.4	24.112	1.867	1.3871	0.3334
Sep. 27	80	0.757050	0.546569	19.316	184.5	21.821	1.824	1.1708	0.3433
Sep. 17	90	0.710614	0.509795	15.637	174.8	20.572	1.800	1.0729	0.3483
Sep. 7	100	0.688659	0.492706	13.437	165.0	20.152	1.788	1.0280	0.3494
Aug. 28	110	0.679270	0.489704	12.072	155.3	20.427	1.782	1.0119	0.3466
Aug. 18	120	0.677063	0.497429	11.241	145.7	21.315	1.781	1.0139	0.3403
Aug. 8	130	0.679284	0.513939	10.796	136.1	22.778	1.782	1.0284	0.3302
Jul. 29	140	0.684401	0.538234	10.665	126.5	24.812	1.785	1.0528	0.3160
Jul. 19	150	0.691526	0.569944	10.828	117.0	27.445	1.789	1.0857	0.2974
Jul. 9	160	0.700134	0.609095	11.305	107.4	30.738	1.794	1.1266	0.2737
Jun. 29	170	0.709934	0.655860	12.167	97.9	34.786	1.800	1.1756	0.2443
Jun 19	180	0.720793	0.710192	13.563	88.3	39.712	1.806	1.2327	0.2089
May 30	200	0.745776	0.836113	19.467	69.2	52.742	1.819	1.3693	0.1222
May 10	220	0.776194	0.949784	40.047	49.9	69.541	1.833	1.5134	0.0390
Apr. 20	240	0.689536	0.970599	59.102	210.6	-74.944	1.788	1.3588	0.0203
Mar. 31	260	0.728581	0.873083	23.174	190.9	-57.695	1.810	1.3647	0.0925

Table 3

STRAIGHT BALLISTIC MISSIONS TO ENCKE IN 1980

ARRIVING AT PERIHELION

Launch Date	Flight Time (Days)	Semi-Major Axis (AU)	Eccentricity	Inclination (DEG)	Node (DEG)	Final γ (DEG)	Final V (EMOS)	Aphelion (AU)	Perihelion (AU)
Oct. 27 (1980)	40	1.047474	.968165	1.524	34.2	7.512	2.408	2.0616	0.0333
Oct. 7	60	.846069	.599697	2.191	14.4	2.205	2.171	1.3535	0.3387
Sep. 27	70	.739137	.541152	2.979	4.5	1.173	2.131	1.1391	0.3392
Sep. 17	80	.696366	.512860	4.857	354.8	0.909	2.111	1.0535	0.3392
Sep. 12	85	.685673	.505304	7.199	349.9	1.002	2.106	1.0321	0.3392
Sep. 7	90	.679194	.500689	13.972	345.0	1.206	2.103	1.0193	0.3391
Sep. 4	93	.676811	.499005	30.919	342.1	1.331	2.101	1.0145	0.3391
Sep. 2	95	.675729	.498123	84.149	340.2	1.193	2.101	1.0123	0.3391
Aug. 31	97	.674998	.498103	34.348	158.2	1.923	2.100	1.0112	0.3388
Aug. 28	100	.674476	.497901	14.723	155.3	2.122	2.100	1.0103	0.3387
Aug. 23	105	.674880	.498765	7.421	150.5	2.638	2.100	1.0115	0.3383
Jul. 29	130	.691034	.518270	2.237	126.5	6.538	2.109	1.0492	0.3329
Jul. 9	150	.711962	.547722	1.555	107.4	10.929	2.119	1.1019	0.3220
Jun. 19	170	.735552	.589226	1.302	88.3	16.469	2.129	1.1690	0.3021

Table 4

STRAIGHT BALLISTIC MISSIONS TO ENCKE IN 1980
ARRIVING 10 DAYS BEFORE PERIHELION

Launch Date	Flight Time (Days)	Semi-Major Axis (AU)	Eccentricity	Inclination (DEG)	Node (DEG)	Final γ (DEG)	Final V (EMOS)	Aphelion (AU)	Perihelion (AU)
Oct. 17 (1980)	40	1.456875	0.725130	9.802	203.8	-15.571	1.969	2.5133	0.4005
Oct. 7	50	0.911224	0.570212	9.585	193.9	-16.011	1.862	1.4308	0.3916
Sep. 27	60	0.775771	0.502226	9.653	184.0	-16.159	1.810	1.1654	0.3862
Sep. 17	70	0.725532	0.469749	10.009	174.3	-15.958	1.785	1.0663	0.3847
Sep. 7	80	0.706434	0.452715	10.703	164.5	-15.444	1.775	1.0262	0.3866
Aug. 28	90	0.701727	0.442998	11.851	154.8	-14.675	1.772	1.0126	0.3909
Aug. 18	100	0.704548	0.437203	13.680	145.2	-13.710	1.774	1.0126	0.3965
Aug. 8	110	0.711585	0.433909	16.677	135.6	-12.603	1.778	1.0203	0.4028
Jul. 29	120	0.721059	0.432614	21.984	126.0	-11.421	1.783	1.0330	0.4091
Jul. 19	130	0.731946	0.433496	32.842	116.5	-10.289	1.789	1.0492	0.4147
Jul. 9	140	0.743626	0.438345	59.899	106.9	-9.649	1.795	1.0696	0.4177
Jun. 29	150	0.755705	0.424491	67.934	277.4	-3.777	1.800	1.0765	0.4349
Jun. 19	160	0.767945	0.432354	35.934	267.9	-3.148	1.806	1.1000	0.4359
Jun. 9	170	0.780184	0.439193	23.342	258.3	-1.628	1.812	1.1228	0.4375
May 20	190	0.804309	0.456713	14.101	239.1	2.316	1.823	1.1716	0.4370
Apr. 30	210	0.827728	0.483222	10.865	219.8	7.114	1.832	1.2277	0.4278
Apr. 10	230	0.850464	0.522950	9.692	200.3	12.946	1.841	1.2959	0.4057
Mar. 21	250	0.872814	0.581914	9.745	180.5	20.308	1.849	1.3807	0.3649
Mar. 1	270	0.895389	0.668389	11.108	160.6	30.101	1.857	1.4939	0.2969
Feb. 10	290	0.788510	0.776015	165.016	320.4	-45.247	1.816	1.4004	0.1766

Table 5

STRAIGHT BALLISTIC MISSIONS TO ENCKE IN 1980
ARRIVING 20 DAYS BEFORE PERIHELION

Launch Date	Flight Time (Days)	Semi-Major Axis (AU)	Eccentricity	Inclination (DEG)	Node (DEG)	Final γ (DEG)	Final V (EMOS)	Aphelion (AU)	Perihelion (AU)
Oct. 7 (1980)	40	1.129078	0.527876	13.929	193.9	-17.417	1.539	1.7251	0.5331
Oct. 2	45	0.979432	0.461300	13.284	189.0	-17.046	1.494	1.4312	0.5276
Sep. 27	50	0.897488	0.417612	12.785	184.0	-16.774	1.463	1.2723	0.5227
Sep. 17	60	0.816814	0.368391	12.134	174.3	-16.351	1.425	1.1177	0.5159
Sep. 7	70	0.783519	0.344026	11.865	164.5	-15.932	1.406	1.0531	0.5140
Aug. 28	80	0.770710	0.330152	11.933	154.8	-15.437	1.399	1.0252	0.5163
Aug. 18	90	0.768262	0.321008	12.343	145.2	-14.845	1.397	1.0149	0.5216
Aug. 8	100	0.771512	0.314271	13.149	135.6	-14.161	1.399	1.0140	0.5290
Jul. 29	110	0.778030	0.309014	14.478	126.0	-13.400	1.403	1.0185	0.5376
Jul. 19	120	0.786435	0.304912	16.582	116.5	-12.584	1.408	1.0262	0.5466
Jul. 9	130	0.795900	0.301949	19.972	106.9	-11.741	1.413	1.0362	0.5556
Jun. 29	140	0.805910	0.300385	25.794	97.4	-10.918	1.419	1.0480	0.5638
Jun. 19	150	0.816138	0.301050	36.957	87.9	-10.231	1.424	1.0618	0.5704
Jun. 9	160	0.826374	0.306820	61.135	78.3	-10.047	1.430	1.0799	0.5728
May 20	180	0.846375	0.281784	44.028	239.1	-3.946	1.440	1.0849	0.6079
Apr. 30	200	0.865376	0.291825	21.676	219.8	-2.032	1.449	1.1179	0.6128
Apr. 10	220	0.883235	0.304503	15.031	200.3	0.811	1.457	1.1522	0.6143
Mar. 21	240	0.900037	0.325183	12.503	180.5	4.332	1.464	1.1927	0.6074
Mar. 1	260	0.916022	0.359325	11.853	160.6	8.785	1.471	1.2452	0.5869
Feb. 10	280	0.931603	0.416543	12.690	140.4	14.799	1.477	1.3197	0.5436
Jan. 21	300	0.947543	0.515399	15.669	120.1	23.747	1.483	1.4359	0.4592
Jan. 1	320	0.965581	0.685628	24.050	99.7	38.609	1.490	1.6276	0.3036

STRAIGHT BALLISTIC MISSIONS TO ENCKE IN 1980

ARRIVING 10 DAYS AFTER PERIHELION

TITAN III D/CENTAUR/TE364(2250)

Launch Date	Julian (244-)	Flight Time (Days)	Payload (KG)	Intercept Speed (KM/SEC)	Departure V_{∞} (KM/SEC)	Departure Declination (DEG)
Oct 2 (1980)	4515	75	Negative	14.674	18.281	9.1
Sep 27	4510	80	88	12.676	16.007	9.2
Sep 22	4505	85	227	11.476	14.178	9.2
Sep 17	4500	90	412	10.772	12.720	9.2
Sep 12	4495	95	619	10.355	11.588	8.9
Sep 7	4490	100	819	10.091	10.751	8.3
Sep 2	4485	105	981	9.898	10.183	7.4
Aug 28	4480	110	1083	9.733	9.861	6.1
Aug 23	4475	115	1116	9.578	9.761	4.6
Aug 18	4470	120	1086	9.432	9.852	2.9
Aug 13	4465	125	1004	9.309	10.108	1.3
Aug 8	4460	130	888	9.233	10.501	-0.3
Aug 3	4455	135	753	9.238	11.009	-1.8
Jul 29	4450	140	614	9.367	11.616	-3.0
Jul 24	4445	145	480	9.665	12.307	-4.1
Jul 19	4440	150	359	10.176	13.077	-4.9
Jul 14	4435	155	254	10.939	13.920	-5.6
Jul 9	4430	160	168	11.981	14.836	-5.9
Jul 4	4425	165	98	13.319	15.827	-6.1
Jun 29	4420	170	45	14.965	16.897	-6.1
Jun 24	4415	175	6	16.925	18.051	-5.8
Jun 19	4410	180	Negative	19.207	19.297	-5.3
May 30	4390	200	Negative	31.727	25.338	-1.1
Apr 30	4360	230	Negative	59.830	37.400	11.1
Mar 21	4320	270	Negative	70.744	25.075	4.4

STRAIGHT BALLISTIC MISSIONS TO ENCKE IN 1980 (cont)

ARRIVING 10 DAYS AFTER PERIHELION

TITAN III D/CENTAUR/TE364(2250)

Launch Date	Julian (244-)	Flight Time (Days)	Payload (KG)	Intercept Speed (KM/SEC)	Departure V ∞ (KM/SEC)	Departure Declination (DEG)
Feb 10	4280	310	Negative	68.459	20.228	15.1
Jan 21	4260	330	8	61.900	17.980	11.9
Jan 1	4240	350	73	55.929	16.295	5.3
Dec 12 (1979)	4220	370	114	51.300	15.578	-6.1
Nov 22	4200	390	21	51.246	17.561	-25.2
Nov 2	4180	410	Negative	81.462	35.187	-46.3
Sep 23	4140	450	Negative	11.546	24.954	3.5
Sep 3	4120	470	212	20.881	14.336	2.6
Aug 14	4100	490	Negative	23.947	29.719	10.0
Jul 25	4080	510	50	10.497	16.781	-9.2
Jun 15	4040	550	Negative	17.630	28.487	-10.8

Table 7

STRAIGHT BALLISTIC MISSIONS TO ENCKE IN 1980

ARRIVING AT PERIHELION

TITAN III D/CENTAUR/TE364(2250)

Launch Date	Julian (244-)	Flight Time (Days)	Payload (KG)	Intercept Speed (KM/SEC)	Departure V^∞ (KM/SEC)	Departure Declination (DEG)
Oct 12 (1980)	4525	55	Negative	16.611	19.977	-17.4
Oct 7	4520	60	36	16.891	17.122	-18.1
Oct 2	4515	65	170	17.344	14.811	-19.2
Sep 27	4510	70	375	17.965	12.962	-20.8
Sep 22	4505	75	633	18.836	11.527	-23.4
Sep 17	4500	80	890	20.204	10.494	-27.2
Sep 12	4495	85	1041	22.823	9.959	-33.6
Sep 7	4490	90	779	30.277	10.775	-47.0
Sep 2	4485	95	Negative	98.275	34.490	-58.1
Aug 28	4480	100	856	8.018	10.614	8.7
Aug 23	4475	105	1347	9.208	9.122	-4.4
Aug 18	4470	110	1404	11.299	8.976	-10.3
Aug 13	4465	115	1343	12.633	9.131	-13.4
Aug 8	4460	120	1236	13.628	9.417	-15.4
Aug 3	4455	125	1110	14.480	9.779	-16.6
Jul 29	4450	130	979	15.288	10.190	-17.4
Jul 24	4445	135	850	16.104	10.636	-17.9
Jul 19	4440	140	729	16.961	11.107	-18.1
Jul 14	4435	145	617	17.880	11.600	-18.1
Jul 9	4430	150	515	18.877	12.112	-18.0
Jul 4	4425	155	424	19.962	12.642	-17.7
Jun 29	4420	160	343	21.143	13.190	-17.2
Jun 24	4415	165	272	22.427	13.758	-16.6
Jun 19	4410	170	211	23.821	14.349	-15.8
Jun 14	4405	175	157	25.330	14.964	-14.9
Jun 9	4400	180	112	26.960	15.607	-13.9
Jun 4	4395	185	73	28.718	16.281	-12.8
May 30	4390	190	41	30.612	16.991	-11.5
May 25	4385	195	15	32.648	17.741	-10.1
May 20	4380	200	Negative	34.835	18.537	-8.6

Table 8

STRAIGHT BALLISTIC MISSIONS TO ENCKE IN 1980

ARRIVING 10 DAYS BEFORE PERIHELION

T III D/CENTAUR/TE364(2250)

Launch Date	Julian (244-)	Flight Time (Days)	Payload (KG)	Intercept Speed (KM/SEC)	Departure V_{∞} (KM/SEC)	Departure Declination (DEG)
Oct 17 (1980)	4530	40	Negative	14.954	24.057	-4.2
Oct 12	4525	45	Negative	14.402	20.298	-3.0
Oct 7	4520	50	28	14.077	17.341	-1.7
Oct 2	4515	55	154	13.874	15.003	-0.3
Sep 27	4510	60	347	13.747	13.165	1.1
Sep 22	4505	65	587	13.680	11.742	2.6
Sep 17	4500	70	840	13.669	10.675	4.1
Sep 12	4495	75	1066	13.720	9.914	5.5
Sep 7	4490	80	1235	13.840	9.420	7.0
Sep 2	4485	85	1333	14.041	9.156	8.3
Aug 28	4480	90	1358	14.339	9.093	9.7
Aug 23	4475	95	1315	14.754	9.205	11.0
Aug 18	4470	100	1214	15.319	9.478	12.5
Aug 13	4465	105	1066	16.082	9.912	14.2
Aug 8	4460	110	880	17.122	10.527	16.1
Aug 3	4455	115	667	18.571	11.371	18.4
Jul 29	4450	120	440	20.656	12.542	21.1
Jul 24	4445	125	223	23.793	14.226	24.0
Jul 19	4440	130	51	28.750	16.769	27.1
Jul 9	4430	140	Negative	50.419	27.268	30.0
Jun 29	4420	150	Negative	69.429	30.353	-49.6
Jun 19	4410	160	Negative	45.648	18.673	-54.5
Jun 9	4400	170	175	37.125	14.618	-48.6
May 20	4380	190	365	33.926	13.007	-33.5
Apr 30	4360	210	287	36.114	13.633	-21.3
Apr 10	4340	230	145	40.547	15.127	-11.1
Mar 21	4320	250	24	46.865	17.452	-2.0
Mar 1	4300	270	Negative	55.517	20.964	6.0
Jan 21	4260	310	Negative	68.016	44.782	24.4
Dec 12 (1979)	4220	350	Negative	53.798	40.576	16.8
Nov 2	4180	390	Negative	32.832	27.479	3.4

Table 9

STRAIGHT BALLISTIC MISSIONS TO ENCKE IN 1980

ARRIVING 20 DAYS BEFORE PERIHELION

T III D/CENTAUR/TE364(2250)

Launch Date	Julian (244-)	Flight Time (Days)	Payload (KG)	Intercept Speed (KM/SEC)	Departure V ∞ (KM/SEC)	Departure Declination (DEG)
Oct 7 (1980)	4520	40	23	19.957	17.487	9.9
Oct 2	4515	45	153	19.997	15.024	11.5
Sep 27	4510	50	357	20.070	13.090	13.2
Sep 22	4505	55	624	20.155	11.566	15.0
Sep 17	4500	60	925	20.253	10.372	16.8
Sep 12	4495	65	1224	20.366	9.450	18.5
Sep 7	4490	70	1492	20.499	8.758	20.1
Sep 2	4485	75	1709	20.657	8.261	21.4
Aug 28	4480	80	1863	20.843	7.931	22.6
Aug 23	4475	85	1955	21.061	7.744	23.6
Aug 18	4470	90	1988	21.315	7.678	24.4
Aug 13	4465	95	1968	21.608	7.719	25.2
Aug 8	4460	100	1901	21.946	7.854	25.9
Aug 3	4455	105	1794	22.333	8.077	26.6
Jul 29	4450	110	1651	22.779	8.389	27.5
Jul 24	4445	115	1477	23.299	8.795	28.6
Jul 19	4440	120	1272	23.911	9.314	29.9
Jul 14	4435	125	1042	24.648	9.971	31.4
Jul 9	4430	130	796	25.560	10.812	33.2
Jun 29	4420	140	312	28.301	13.375	37.6
Jun 19	4410	150	Negative	33.793	18.278	42.2
Jun 9	4400	160	Negative	46.531	28.524	43.7
May 30	4390	170	Negative	58.548	34.500	-38.1
May 20	4380	180	Negative	42.274	21.634	-48.2
Apr 30	4360	200	413	33.741	12.607	-45.1
Apr 10	4340	220	822	33.751	10.714	-32.9
Mar 21	4320	240	825	35.740	10.728	-21.2
Mar 1	4300	260	589	38.871	11.734	-11.6
Feb 10	4280	280	270	43.344	13.776	-4.3
Jan 21	4260	300	22	50.050	17.514	0.3
Jan 1	4240	320	Negative	60.926	24.605	1.4
Nov 2	4180	380	Negative	30.750	39.158	4.1

Table 10

STRAIGHT BALLISTIC MISSIONS TO ENCKE IN 1980

ARRIVING 30 DAYS BEFORE PERIHELION

T III D/CENTAUR/TE364(2250)

Launch Date	Julian (244-)	Flight Time (Days)	Payload (KG)	Intercept Speed (KM/SEC)	Departure V^∞ (KM/SEC)	Departure Declination (DEG)
Sep 27 (1980)	4510	40	349	27.546	13.130	32.1
Sep 22	4505	45	625	27.390	11.532	34.0
Sep 17	4500	50	940	27.272	10.272	36.1
Sep 12	4495	55	1265	27.181	9.270	38.2
Sep 7	4490	60	1574	27.111	8.474	40.4
Sep 2	4485	65	1850	27.059	7.845	42.4
Aug 28	4480	70	2080	27.026	7.357	44.3
Aug 23	4475	75	2262	27.013	6.992	46.0
Aug 18	4470	80	2393	27.020	6.733	47.4
Aug 13	4465	85	2477	27.048	6.568	48.5
Aug 8	4460	90	2515	27.098	6.489	49.3
Aug 3	4455	95	2512	27.171	6.489	49.9
Jul 29	4450	100	2467	27.268	6.564	50.2
Jul 24	4445	105	2384	27.392	6.713	50.5
Jul 19	4440	110	2262	27.547	6.939	50.6
Jul 14	4435	115	2101	27.736	7.246	50.8
Jul 9	4430	120	1901	27.968	7.647	51.1
Jul 4	4425	125	1663	28.254	8.159	51.5
Jun 29	4420	130	1390	28.611	8.811	52.1
Jun 19	4410	140	773	29.670	10.724	53.7
Jun 9	4400	150	214	31.674	14.087	55.8
May 20	4380	170	Negative	47.479	33.981	54.1
Apr 30	4360	190	Negative	35.729	18.864	-48.1
Apr 10	4340	210	833	31.658	10.535	-50.2
Mar 21	4320	230	1709	31.617	8.135	-43.9
Mar 1	4300	250	2041	32.487	7.519	-35.6
Feb 10	4280	270	1902	33.922	7.852	-28.1
Jan 21	4260	290	1348	36.109	9.117	-22.7
Jan 1	4240	310	539	39.803	11.984	-20.1
Dec 12 (1979)	4220	330	Negative	47.515	19.005	-20.8
Nov 22	4200	350	Negative	65.727	38.173	-24.8

STRAIGHT BALLISTIC MISSIONS TO ENCKE IN 1980

ARRIVING 40 DAYS BEFORE PERIHELION

T III D/CENTAUR/TE364(2250)

Launch Date	Julian (244-)	Flight Time (Days)	Payload (KG)	Intercept Speed (KM/SEC)	Departure V_{∞} (KM/SEC)	Departure Declination (DEG)
Sep 17 (1980)	4500	40	388	36.142	12.531	58.3
Sep 12	4495	45	592	35.421	11.270	59.5
Sep 7	4490	50	787	34.837	10.275	61.0
Sep 2	4485	55	952	34.347	9.476	62.6
Aug 28	4480	60	1070	33.928	8.827	64.4
Aug 23	4475	65	1135	33.564	8.299	66.3
Aug 18	4470	70	1147	33.242	7.870	68.3
Aug 13	4465	75	1117	32.958	7.527	70.4
Aug 8	4460	80	1055	32.705	7.259	72.6
Aug 3	4455	85	975	32.480	7.060	74.7
Jul 29	4450	90	890	32.282	6.927	76.8
Jul 24	4445	95	810	32.109	6.858	78.7
Jul 19	4440	100	743	31.960	6.854	80.1
Jul 14	4435	105	696	31.835	6.917	81.1
Jul 9	4430	110	671	31.737	7.054	81.3
Jul 4	4425	115	664	31.667	7.273	80.9
Jun 29	4420	120	664	31.630	7.588	79.9
Jun 24	4415	125	656	31.632	8.016	78.6
Jun 19	4410	130	625	31.684	8.587	77.2
Jun 9	4400	140	452	32.021	10.340	74.6
May 30	4390	150	157	32.986	13.523	72.6
May 20	4380	160	Negative	35.707	19.896	70.8
Apr 30	4360	180	Negative	41.523	31.746	-36.0
Apr 10	4340	200	337	31.595	13.075	-52.0
Mar 21	4320	220	1547	30.218	8.254	-56.2
Mar 1	4300	240	2213	29.888	6.518	-58.4
Feb 10	4280	260	2382	29.853	5.951	-59.5
Jan 21	4260	280	2272	30.013	6.149	-59.9
Jan 1	4240	300	1803	30.466	7.257	-60.0

STRAIGHT BALLISTIC MISSIONS TO ENCKE IN 1980 (cont)

ARRIVING 40 DAYS BEFORE PERIHELION

T III D/CENTAUR/TE364(2250)

Launch Date	Julian (244-)	Flight Time (Days)	Payload (KG)	Intercept Speed (KM/SEC)	Departure V ∞ (KM/SEC)	Departure Declination (DEG)
Dec 12 (1979)	4220	320	788	31.710	10.284	-60.8
Nov 22	4200	340	Negative	36.963	20.487	-62.8
Nov 2	4180	360	Negative	37.009	30.599	36.2
Oct 13	4160	380	402	29.063	12.624	51.5
Sep 23	4140	400	1641	28.468	8.037	56.0
Sep 3	4120	420	2282	28.479	6.369	58.4
Aug 14	4100	440	2432	28.588	5.799	59.7
Jul 25	4080	460	2332	28.735	5.920	60.3
Jul 5	4060	480	1991	28.888	6.805	59.9
May 26	4020	520	49	32.997	15.914	68.1
May 6	4000	540	Negative	47.931	41.196	-26.4
71 Apr 16	3980	560	100	31.889	15.655	-51.1
Mar 27	3960	580	1238	29.844	9.052	-56.6
Mar 7	3940	600	2072	29.507	6.827	-58.4
Feb 15	3920	620	2387	29.529	6.032	-59.0
Jan 26	3900	640	2377	29.734	6.043	-59.1
Jan 6	3880	660	2007	30.171	6.872	-59.2
Dec 17 (1978)	3860	680	1104	31.172	9.197	-60.1

STRAIGHT BALLISTIC MISSIONS TO ENCKE IN 1980

ARRIVING ONE DAY AFTER PERIHELION

TITAN III D/CENTAUR/TE364(2250)

Launch Date	Flight Time (Days)	Payload (KG)	Intercept Speed (KM/SEC)	Departure V_{∞} (KM/SEC)	Departure Declination (DEG)
	92.0	Negative	38.284	21.054	23.3
	92.5	Negative	33.023	19.270	23.2
	93.0	13	28.625	17.790	22.7
	93.5	60	24.946	16.563	22.0
	94.0	116	21.857	15.541	21.0
	94.5	180	19.254	14.686	20.0
Sep 3 (1980)	95.0	250	17.054	13.965	18.9
	95.5	322	15.190	13.354	17.7
	96.0	395	13.609	12.832	16.6
	96.5	467	12.272	12.385	15.4
	97.0	536	11.144	11.998	14.2
	97.5	603	10.200	11.663	13.1
	98.0	667	9.419	11.372	12.0
	98.5	727	8.781	11.116	11.0
	99.0	782	8.272	10.892	9.9
	99.5	834	7.875	10.694	9.0
Aug 29	100.0	882	7.578	10.520	8.0
	100.5	927	7.367	10.365	7.1
	101.0	967	7.230	10.228	6.2
	101.5	1004	7.154	10.107	5.4
	102.0	1038	7.129	9.999	4.6
	102.5	1069	7.147	9.903	3.8
	103.0	1097	7.197	9.817	3.1
	103.5	1123	7.273	9.742	2.4
	104.0	1145	7.370	9.674	1.7
	104.5	1166	7.483	9.615	1.0

STRAIGHT BALLISTIC MISSIONS TO ENCKE IN 1980 (cont)

ARRIVING ONE DAY AFTER PERIHELION

TITAN III D/CENTAUR/TE364(2250)

Launch Date	Flight Time (Days)	Payload (KG)	Intercept Speed (KM/SEC)	Departure V_{∞} (KM/SEC)	Departure Declination (DEG)
Aug 24	105.0	1184	7.607	9.563	0.4
	105.5	1200	7.739	9.517	-0.2
	106.0	1215	7.877	9.477	-0.8
	106.5	1227	8.019	9.443	-1.3
	107.0	1238	8.164	9.413	-1.9
	107.5	1249	8.309	9.388	-2.4
	108.0	1255	8.455	9.367	-2.9
	108.5	1261	8.600	9.350	-3.3
	109.0	1266	8.744	9.336	-3.8
	109.5	1269	8.887	9.326	-4.2
Aug 19	110.0	1272	9.028	9.319	-4.7
	110.5	1274	9.167	9.315	-5.1
	111.0	1274	9.304	9.314	-5.5
	111.5	1274	9.438	9.315	-5.9
	112.0	1272	9.571	9.319	-6.2
	112.5	1270	9.701	9.324	-6.6
	113.0	1267	9.829	9.333	-6.9
	113.5	1263	9.955	9.343	-7.3
	114.0	1259	10.079	9.354	-7.6
	114.5	1254	10.201	9.368	-7.9
Aug 14	115.0	1248	10.320	9.384	-8.2
	115.5	1242	10.438	9.401	-8.5
	116.0	1235	10.554	9.419	-8.7

STRAIGHT BALLISTIC MISSIONS TO ENCKE IN 1980

ARRIVING AT PERIHELION

TITAN III D/CENTAUR/TE364(2250)

Launch Date	Flight Time (Days)	Payload (KG)	Intercept Speed (KM/SEC)	Departure V_{∞} (KM/SEC)	Departure Declination (DEG)	
Sep 12 (1980)	85.0	1041	22.823	9.959	-33.6	
	85.5	1043	23.229	9.947	-34.5	
	86.0	1041	23.678	9.947	-35.4	
	86.5	1034	24.178	9.960	-36.5	
	87.0	1022	24.738	9.989	-37.6	
	87.5	1004	25.369	10.037	-38.9	
	88.0	979	26.085	10.109	-40.2	
	88.5	946	26.906	10.209	-41.7	
	89.0	902	27.855	10.345	-43.3	
	89.5	847	28.964	10.529	-45.1	
	Sep 7	90.0	779	30.277	10.775	-47.0
		90.5	694	31.854	11.103	-49.2
		91.0	593	33.780	11.546	-51.5
		91.5	473	36.178	12.149	-54.1
92.0		334	39.234	12.986	-56.8	
92.5		193	43.231	14.169	-59.5	
93.0		70	48.618	15.882	-62.1	
93.5		Negative	56.092	18.418	-64.2	
94.0		Negative	66.644	22.210	-64.9	
94.5		Negative	81.114	27.682	-63.2	
Sep 2	95.0	Negative	98.275	34.490	-58.1	
	95.5	Negative	68.273	31.153	18.5	
	96.0	Negative	49.772	24.824	22.6	
	96.5	Negative	36.088	20.163	23.6	
	97.0	41	26.663	17.004	22.6	
	97.5	165	20.189	14.873	20.5	
	98.0	315	15.682	13.404	18.1	
	98.5	470	12.525	12.364	15.6	
	99.0	615	10.345	11.607	13.1	
	99.5	745	8.899	11.043	10.8	

STRAIGHT BALLISTIC MISSIONS TO ENCKE IN 1980 (cont)

ARRIVING AT PERIHELION

TITAN III D/CENTAUR/TE364(2250)

Launch Date	Flight Time (Days)	Payload (KG)	Intercept Speed (KM/SEC)	Departure V_{∞} (KM/SEC)	Departure Declination (DEG)
Aug 28	100.0	856	8.018	10.614	8.7
	100.5	951	7.558	10.282	6.8
	101.0	1031	7.398	10.020	5.0
	101.5	1099	7.436	9.812	3.4
	102.0	1156	7.596	9.645	2.0
	102.5	1203	7.826	9.509	0.7
	103.0	1243	8.093	9.398	-0.5
	103.5	1276	8.374	9.308	-1.6
	104.0	1304	8.658	9.233	-2.7
	104.5	1327	8.938	9.172	-3.6
Aug 23	105.0	1347	9.208	9.122	-4.4
	105.5	1362	9.467	9.081	-5.2
	106.0	1375	9.714	9.049	-5.9
	106.5	1385	9.949	9.023	-6.6
	107.0	1393	10.173	9.003	-7.3
	107.5	1399	10.385	8.989	-7.8
	108.0	1403	10.586	8.979	-8.4
	108.5	1405	10.778	8.973	-8.9
	109.0	1406	10.960	8.971	-9.4
	109.5	1405	11.133	8.972	-9.8
Aug 18	110.0	1404	11.299	8.976	-10.3
	110.5	1401	11.457	8.982	-10.7
	111.0	1398	11.609	8.991	-11.0
	111.5	1393	11.754	9.003	-11.4
	112.0	1388	11.893	9.016	-11.7
	112.5	1382	12.028	9.031	-12.1
	113.0	1375	12.157	9.048	-12.4
	113.5	1368	12.282	9.066	-12.7
	114.0	1360	12.403	9.087	-12.9
	114.5	1352	12.519	9.108	-13.2
115.0	1343	12.633	9.131	-13.4	

STRAIGHT BALLISTIC MISSIONS TO ENCKE IN 1980

ARRIVING ONE DAY BEFORE PERIHELION

TITAN III D/CENTAUR/TE364(2250)

Launch Date	Flight Time (Days)	Payload (KG)	Intercept Speed (KM/SEC)	Departure V_{∞} (KM/SEC)	Departure Declination (DEG)
	84.0	1230	14.892	9.434	-17.3
	84.5	1254	14.882	9.368	-17.4
Sep 11 (1980)	85.0	1278	14.871	9.304	-17.4
	85.5	1301	14.859	9.242	-17.5
	86.0	1323	14.846	9.184	-17.5
	86.5	1345	14.831	9.127	-17.5
	87.0	1365	14.815	9.074	-17.6
	87.5	1385	14.798	9.023	-17.6
	88.0	1404	14.778	8.975	-17.6
	88.5	1423	14.757	8.929	-17.6
	89.0	1440	14.733	8.885	-17.6
	89.5	1457	14.707	8.844	-17.6
Sep 6	90.0	1473	14.678	8.806	-17.6
	90.5	1488	14.645	8.770	-17.6
	91.0	1502	14.609	8.736	-17.6
	91.5	1515	14.568	8.704	-17.5
	92.0	1527	14.521	8.675	-17.5
	92.5	1538	14.469	8.649	-17.4
	93.0	1549	14.409	8.624	-17.3
	93.5	1558	14.341	8.603	-17.2
	94.0	1566	14.261	8.583	-17.0
	94.5	1573	14.169	8.566	-16.8
Sep 1	95.0	1579	14.060	8.553	-16.6
	95.5	1584	13.930	8.542	-16.3
	96.0	1587	13.774	8.535	-15.9
	96.5	1588	13.581	8.532	-15.5
	97.0	1587	13.340	8.535	-14.9
	97.5	1583	13.030	8.545	-14.1
	98.0	1572	12.619	8.569	-13.1
	98.5	1553	12.053	8.614	-11.6
	99.0	1515	11.232	8.703	-9.4

STRAIGHT BALLISTIC MISSIONS TO ENCKE IN 1980 (cont)

ARRIVING ONE DAY BEFORE PERIHELION

TITAN III D/CENTAUR/TE364(2250)

Launch Date	Flight Time (Days)	Payload (KG)	Intercept Speed (KM/SEC)	Departure V_{∞} (KM/SEC)	Departure Declination (DEG)	
Aug 27	99.5	1435	9.978	8.899	-5.8	
	100.0	1226	8.183	9.445	0.8	
	100.5	550	11.657	11.929	14.4	
	101.0	Negative	95.708	33.435	-58.3	
	101.5	615	34.521	11.391	-54.4	
	102.0	1221	25.480	9.360	-42.1	
	102.5	1420	22.282	8.883	-36.0	
	103.0	1501	20.673	8.709	-32.7	
	103.5	1540	19.711	8.631	-30.6	
	104.0	1561	19.076	8.593	-29.1	
	104.5	1570	18.628	8.575	-28.1	
	Aug 22	105.0	1573	18.297	8.568	-27.3
		105.5	1572	18.045	8.569	-26.7
		106.0	1570	17.846	8.574	-26.2
106.5		1567	17.688	8.582	-25.9	
107.0		1562	17.560	8.594	-25.5	
107.5		1556	17.455	8.607	-25.3	
108.0		1549	17.369	8.623	-25.0	
108.5		1542	17.297	8.640	-24.8	
109.0		1534	17.237	8.658	-24.7	
109.5		1526	17.187	8.678	-24.5	
Aug 17	110.0	1517	17.146	8.699	-24.4	
	110.5	1508	17.112	8.721	-24.3	
	111.0	1498	17.084	8.744	-24.2	
	111.5	1488	17.062	8.767	-24.1	
	112.0	1478	17.044	8.792	-24.0	
	112.5	1468	17.031	8.818	-23.9	
	113.0	1457	17.021	8.844	-23.8	
	113.5	1446	17.015	8.872	-23.8	
	114.0	1434	17.012	8.900	-23.7	

VENUS SWINGBY MISSIONS TO ENCKE IN 1980

Julian Date at Venus (-2440000)

	4438	4439	4440	4441	4442	
4285	1.14 8.39 175	NONE		<u>NOTE</u> Parameters shown are: upper - passage distance (Venus radii) center - launch excess (km/sec) lower - Venus-Encke flight time (days)		
4286	1.54 7.81 174	NONE				
4287	1.98 7.32 173	1.19 8.20 174	NONE			
4288	2.37 6.91 172	1.58 7.65 173	NONE		NONE	
4289	2.56 6.56 171	2.02 7.19 172	1.25 8.02 173		NONE	
4290	2.44 6.25 170	2.40 6.80 171	1.64 7.50 172		NONE	
4291	2.00/1.18 5.98 169/166	2.60 6.46 170	2.06 7.06 171		1.30 7.84 172	NONE

Julian Date at Earth (-2440000)

VENUS SWINGBY MISSIONS TO ENCKE IN 1980

Julian Date at Venus (-2440000)

64
Julian Date at Earth (-2440000)

	4438	4439	4440	4441	4442	4443	4444	4445
4291	2.00/1.18 5.98 169/166	2.60 6.46 170	2.06 7.06 171	1.30 7.84 172	NONE			
4292		2.50 6.16 169	2.44 6.69 170	1.69 7.36 171	1.04 8.22 172	NONE	NONE	NONE
4293		NONE	2.61 6.26 169	2.29 6.81 170	1.36 7.68 171	NONE	NONE	NONE
4294		NONE	2.37/1.09 5.98 168/163	2.59 6.47 169	1.75 7.21 170	1.09 8.03 171	NONE	NONE
4295		NONE	NONE	2.66 6.16 168	2.17 6.82 169	1.43 7.52 170	NONE	NONE
4296			NONE	2.41/1.16 5.90 167/162	2.54 6.47 168	1.82 7.08 169	1.16 7.85 169	NONE
4297			NONE	NONE	2.72 6.17 167	2.23 6.70 168	1.50 7.36 168	NONE

VENUS SWINGBY MISSIONS TO ENCKE IN 1980

Julian Date at Venus (-2440000)

08
Julian Date at Earth (-2440000)

	4442	4443	4444	4445	4446	4447	4448	4449
4297	2.72 6.17 167	2.23 6.70 168	1.50 7.36 168	NONE	NONE	NONE		
4298	2.62/1.14 5.90 166/161	2.59 6.37 167	1.89 6.95 167	1.23 7.68 168	NONE	NONE		
4299	2.09/1.80 5.66 164/163	2.76/1.00 6.08 166/159	2.30 6.58 166	1.57 7.22 167	1.00 8.02 168	NONE		
4300	NONE	2.63/1.25 5.82 164/160	2.64 6.26 165	1.97 6.82 166	1.30 7.51 167	NONE	NONE	
4301	NONE	NONE	2.79/1.09 5.99 164/158	2.38 6.47 165	1.65 7.07 166	1.07 7.83 167	NONE	NONE
4302		NONE	2.62/1.38 5.74 163/159	2.70 6.17 164	2.06 6.69 165	1.38 7.35 166	NONE	NONE
4303		NONE	NONE	2.81/1.20 5.90 163/157	2.46 6.36 164	1.74 6.93 165	1.14 7.65 166	NONE

VENUS SWINGBY MISSIONS TO ENCKE IN 1980

Julian Date at Venus (-2440000)

	4445	4446	4447	4448	4449	4450	4451	4452
4303	2.81/1.20 5.90 163/157	2.46 6.36 164	1.74 6.93 165	1.14 7.65 166	NONE	NONE		
4304	2.57/1.55 5.66 162/158	2.76/1.09 6.07 163/155	2.15 6.57 164	1.46 7.20 164	NONE	NONE		
4305	NONE	2.82/1.34 5.81 162/156	2.54/1.00 6.26 163/153	1.84 6.80 163	1.22 7.48 164	NONE	NONE	
4306	NONE	2.44/2.04 5.58 160/159	2.81/1.21 5.98 162/155	2.25 6.46 162	1.56 7.05 163	1.02 7.79 164	NONE	NONE
4307		NONE	2.81/1.51 5.73 160/156	2.63/1.11 6.16 161/153	1.94 6.67 162	1.31 7.32 163	NONE	NONE
4308			NONE	2.86/1.35 5.89 160/154	2.36/1.03 6.35 161/151	1.66 6.91 162	1.10 7.60 163	NONE
4309			NONE	2.75/1.74 5.65 159/155	2.72/1.24 6.06 160/152	2.06 6.55 161	1.41 7.16 162	NONE

VENUS SWINGBY MISSIONS TO ENCKE IN 1980

Julian Date at Venus (-2440000)

	4448	4449	4450	4451	4452
4309	2.75/1.74 5.65 159/155	2.72/1.24 6.06 160/152	2.06 6.55 161	1.41 7.16 162	NONE
4310	NONE	2.89/1.54 5.80 159/153	2.47/1.15 6.24 160/151	1.77 6.77 160	1.19 7.43 161
4311		2.67 5.58 157	2.80/1.40 5.96 157/152	2.18/1.08 6.43 159/149	1.51 7.01 160
4312		NONE	2.87/1.79 5.72 157/153	2.58/1.30 6.14 158/150	1.89/1.01 6.64 159/147
4313			NONE	2.87/1.61 5.87 157/151	2.31/1.22 6.32 158/148
4314				2.71/2.42 5.64 155/154	2.70/1.49 6.04 157/150
4315				NONE	2.90/1.89 5.79 155/151
4316					NONE

Julian Date at Earth (-2440000)

Table 16

CHARACTERISTICS OF SELECTED 1984 ENCKE RENDEZVOUS MISSION

Launch date	April 27, 1982 (2445087)
Launch vehicle	Tital III D/Centaur/TE364 (2250)
Reference power	15 kw
Specific impulse	3000 sec
Propulsion system efficiency	0.63585
Specific propulsion system mass	30 kg/kw
Tankage factor	0.03
Maximum power required	17.55 kw
Maximum thrust	0.75861 n
Propulsion time	665 days (continuous)
Flight time	665 days
Launch excess speed	9003 m/sec
Departure asymptote declination	-29.66 deg
Maximum thrust cone angle	175.0 deg
Minimum thrust cone angle	68.8 deg
Maximum solar distance	2.696 AU
Minimum solar distance	0.87487 AU
Arrival communication distance	1.44 AU
Arrival communication angle	36.5 deg
Initial spacecraft mass*	1391 kg
Propulsion system mass	450 kg
Propellant mass	473 kg
Tankage mass	14 kg
Net spacecraft mass	454 kg

*Adjusted for departure asymptote declination greater than 28.5 degrees.

Table 17

0.25 AU $1\frac{1}{2}$ REVOLUTION SOLAR PROBES (SEP)

TITAN III D/CENTAUR/TE364(2250)

OPTIMUM POWER, OPTIMUM VARIABLE THRUST ANGLE, $\alpha = 30\text{KG/KW}$, $I_{SP} = 3000\text{ SEC.}$

Flight Time (Days)	Net Mass (KG)	Reference Power (KW)	Departure V^∞ (KM/SEC)	Travel Angle (DEG)	First Min Distance (AU)	First Max Distance (AU)	Final Semi-Major Axis (AU)	Final Eccentricity
250	1682	28.7	4.853	541.7	0.387	0.730	0.4838	0.4849
240	1565	29.4	5.056	534.2	0.375	0.707	0.4744	0.4771
230	1418	30.7	5.278	524.5	0.360	0.688	0.4659	0.4730
220	1246	31.8	5.561	514.1	0.343	0.671	0.4563	0.4717
210	1057	32.4	5.926	503.0	0.322	0.657	0.4457	0.4753
200	858	32.0	6.401	491.2	0.300	0.645	0.4345	0.4860
190	657	30.2	7.022	478.9	0.276	0.637	0.4230	0.5057
180	463	26.8	7.838	466.2	0.249	0.632	0.4116	0.5353
170	291	21.7	8.917	453.3	0.219	0.631	0.4003	0.5760
160	152	15.3	10.360	440.1	0.186	0.635	0.3896	0.6291

Table 18

0.25 AU $2\frac{1}{2}$ REVOLUTION SOLAR PROBES (SEP)

TITAN III D/CENTAUR/TE364(2250)

OPTIMUM POWER, OPTIMUM VARIABLE THRUST ANGLE, $\alpha = 30$ KG/KW, $I_{SP} = 3000$ SEC

Flight Time (Days)	Net Mass (KG)	Reference Power (KW)	Departure V_{∞} (KM/SEC)	Travel Angle (DEG)	1st Min. Distance (AU)	1st Max. Distance (AU)	2nd Min. Distance (AU)	2nd Max. Distance (AU)	Final Semi-Major Axis (AU)	Final Eccentricity
360	1687	30.6	4.042	885.0	.437	.696	.295	.598	.4225	.4145
350	1583	31.4	4.182	882.7	.426	.690	.284	.577	.4116	.4015
340	1474	32.2	4.334	880.4	.413	.683	.272	.558	.4011	.3902
330	1359	33.1	4.492	876.7	.401	.674	.259	.542	.3917	.3834
320	1236	34.3	4.657	869.4	.388	.663	.250	.531	.3839	.3842
310	1107	35.3	4.859	860.5	.373	.653	.242	.523	.3765	.3892
300	973	35.8	5.115	851.5	.357	.645	.233	.515	.3687	.3972
290	835	35.8	5.433	842.7	.340	.639	.223	.508	.3608	.4087
280	697	35.1	5.825	833.9	.321	.634	.212	.503	.3528	.4244
270	562	33.5	6.309	825.3	.300	.631	.200	.498	.3448	.4450
260	431	31.0	6.910	816.7	.278	.630	.186	.496	.3371	.4712
250	310	27.3	7.661	808.0	.254	.631	.171	.496	.3296	.5041
240	204	22.5	8.610	799.3	.227	.634	.154	.498	.3226	.5449
230	118	16.8	9.822	790.3	.196	.640	.134	.504	.3159	.5947
220	56	10.7	11.392	780.8	.163	.650	.112	.512	.3096	.6548

Table 19

0.25 AU $3\frac{1}{2}$ REVOLUTION SOLAR PROBES (SEP)

TITAN III D/CENTAUR/TE364(2250)

OPTIMUM POWER, OPTIMUM VARIABLE THRUST ANGLE, $\alpha = 30$ KG/KW, $I_{SP} = 3000$ SEC

Flight Time (Days)	Net Mass (KG)	Reference Power (KW)	Departure V_{∞} (KM/SEC)	Travel Angle (DEG)	Minimum Distance (AU)	Maximum Distances (AU)	Final Semi-Major Axis (AU)	Final Eccentricity
480	1861	28.2	3.518	1260	.480/.327/.258	.717/.579/.575	.4120	.3954
470	1796	29.4	3.584	1261	.470/.316/.249	.709/.570/.567	.4080	.3900
460	1726	30.6	3.611	1257	.463/.310/.248	.699/.557/.556	.4021	.3826
450	1651	31.9	3.656	1253	.455/.302/.247	.689/.546/.545	.3964	.3757
440	1570	33.2	3.716	1249	.447/.293/.246	.679/.535/.535	.3905	.3695
430	1485	34.5	3.790	1245	.437/.285/.245	.670/.525/.525	.3846	.3643
98 420	1395	35.7	3.877	1240	.428/.276/.242	.662/.515/.515	.3785	.3609
410	1300	36.8	3.978	1234	.418/.267/.238	.653/.506/.506	.3722	.3603
400	1202	37.8	4.100	1227	.408/.258/.233	.646/.499/.499	.3658	.3630
390	1100	38.5	4.247	1220	.397/.249/.227	.640/.492/.492	.3592	.3691
380	994	39.0	4.425	1213	.385/.240/.219	.634/.486/.486	.3526	.3785
370	887	38.8	4.659	1205	.373/.230/.211	.632/.484/.474	.3428	.3839
360	779	38.2	4.933	1197	.360/.220/.203	.631/.483/.464	.3330	.3923
350	671	37.3	5.250	1189	.346/.209/.193	.630/.483/.456	.3241	.4058
340	564	35.9	5.624	1181	.330/.198/.182	.630/.482/.450	.3159	.4241
330	460	34.0	6.069	1174	.313/.185/.171	.630/.483/.446	.3081	.4473
320	361	31.4	6.606	1167	.294/.172/.158	.632/.485/.444	.3007	.4759
310	269	28.0	7.260	1159	.273/.157/.145	.636/.489/.444	.2938	.5105
300	186	23.8	8.067	1152	.249/.141/.130	.641/.494/.446	.2874	.5518

Table 20

CODE DESCRIPTIONS FOR FOLLOWING PAGES

GENERAL

Titan III D/Centaur/TE364(2250)

$$I_{SP} = 3000 \text{ sec}$$

Optimum Variable Thrust Angle

(P_o is Reference Power)

SPECIFIC

<u>CODE</u>	<u>DESCRIPTION</u>
A	$P_o = \text{Optimum}$
B	$P_o = 15 \text{ kw}$
C	$P_o = 15 \text{ kw}; \text{ Without TE364}$
D	$P_o = 15 \text{ kw}; \text{ Optimum Fixed Thrust Angle}$

Table 21

0.25 AU $1\frac{1}{2}$ REVOLUTION SOLAR PROBES (SEP)

$\alpha = 30 \text{ kg/kw}$

Code	Flight Time (Days)	Net Mass (KG)	Departure V^∞ (km/sec)	Travel Angle (DEG)	1st Min Distance (AU)	1st Max Distance (AU)	Final Semi-Major Axis (AU)	Final Eccentricity
A	250	1682	4.853	541.7	.387	.730	.4838	.4849
B	250	1548	6.574	535.2	.352	.796	.5162	.5176
C	250	1572	6.618	534.9	.351	.798	.5169	.5183
D	250	1541	6.603	531.0	.351	.804	.5198	.5226
A	200	858	6.401	491.2	.300	.645	.4345	.4860
B	200	728	8.533	473.7	.265	.723	.4636	.5610
C	200	699	8.352	473.8	.269	.717	.4611	.5582
D	200	627	8.819	459.4	.250	.758	.4684	.6177
A	180	463	7.838	466.2	.249	.632	.4116	.5353
B	180	413	9.457	455.1	.224	.684	.4290	.5955
C	180	372	9.035	456.5	.232	.672	.4245	.5845
D	180	300	9.850	440.9	.208	.725	.4348	.6667
A	160	152	10.360	440.1	.186	.635	.3896	.6291
B	160	152	10.410	439.8	.185	.636	.3900	.6309
C	160	110	9.633	442.8	.197	.616	.3831	.6077
D	160	41	10.909	428.1	.177	.675	.3976	.6973

$P_o = 28.7 \text{ kw}$

$\theta_T = 94.^\circ 6$

$P_o = 32.0 \text{ kw}$

$\theta_T = 94.^\circ 8$

$P_o = 26.8 \text{ kw}$

$\theta_T = 93.^\circ 6$

$P_o = 15.3 \text{ kw}$

$\theta_T = 91.^\circ 4$

Table 22

0.25 AU $2\frac{1}{2}$ REVOLUTION SOLAR PROBES (SEP) $\alpha = 30$ kg/kw

Code	Flight Time (Days)	Net Mass (KG)	Departure V^∞ (KM/SEC)	Travel Angle (DEG)	Minimum Distances (AU)	Maximum Distances (AU)	Final Semi-Major Axis (AU)	Final Eccentricity
------	--------------------	---------------	-------------------------------	--------------------	------------------------	------------------------	----------------------------	--------------------

A	360	1687	4.042	885.0	.437/.295	.696/.598	.4225	.4145
B	360	1456	6.374	867.5	.372/.269	.782/.657	.4478	.4667
C	360	1475	6.438	866.3	.370/.268	.784/.659	.4486	.4694
D	360	1383	6.558	852.5	.360/.247	.802/.688	.4558	.5090

$P_o = 30.6$ kw

$\theta_T = 92.^\circ_3$

A	320	1236	4.657	869.4	.388/.250	.663/.531	.3839	.3842
B	320	977	7.436	834.8	.317/.217	.754/.622	.4124	.5090
C	320	975	7.421	834.2	.318/.218	.754/.622	.4119	.5096
D	320	860	7.714	818.5	.301/.185	.782/.667	.4197	.5902

$P_o = 34.3$ kw

$\theta_T = 91.^\circ_3$

A	280	697	5.825	833.9	.321/.212	.634/.503	.3528	.4244
B	280	540	8.538	809.0	.264/.167	.718/.581	.3693	.5731
C	280	523	8.339	809.8	.270/.170	.713/.575	.3672	.5650
D	280	402	9.037	795.2	.242/.140	.749/.631	.3810	.6574

$P_o = 35.1$ kw

$\theta_T = 90.^\circ_6$

A	240	204	8.610	799.3	.227/.154	.634/.498	.3226	.5449
B	240	190	9.828	792.5	.205/.138	.664/.526	.3284	.6008
C	240	165	9.231	794.1	.218/.142	.652/.512	.3235	.5834
D	240	60	10.421	781.3	.201/.119	.691/.564	.3380	.6695

$P_o = 22.5$ kw

$\theta_T = 89.^\circ_0$